UNCLASSIFIED
SECURITY CLASSIFICATION OF THIS PAGE

MASTER COPY DTIC FILE COPY FOR REPRODUCTION PURPOSES

RT DOCUMENTATION PAGE

AD-A218 856

1a. R	1b. RESTRICTIVE MARKINGS
2a. S	3. DISTRIBUTION/AVAILABILITY OF REPORT Approved for public release; distribution unlimited.
2b. D	
4. PERFORMING ORGANIZATION REPORT NUMBER(S)	5. MONITORING ORGANIZATION REPORT NUMBER(S) ARO 25822.3-PH
6a. NAME OF PERFORMING ORGANIZATION Duke Univesity	6b. OFFICE SYMBOL (If applicable)
6c. ADDRESS (City, State, and ZIP Code) Durham, North Carolina, 27706	7a. NAME OF MONITORING ORGANIZATION U. S. Army Research Office
	7b. ADDRESS (City, State, and ZIP Code) P. O. Box 12211 Research Triangle Park, NC 27709-2211
8a. NAME OF FUNDING/SPONSORING ORGANIZATION U. S. Army Research Office	8b. OFFICE SYMBOL (If applicable)
8c. ADDRESS (City, State, and ZIP Code) P. O. Box 12211 Research Triangle Park, NC 27709-2211	9. PROCUREMENT INSTRUMENT IDENTIFICATION NUMBER DAAL03-88-C-0014
	10. SOURCE OF FUNDING NUMBERS PROGRAM ELEMENT NO. / PROJECT NO. / TASK NO. / WORK UNIT ACCESSION NO.

11. TITLE (Include Security Classification)
FREQUENCY DOMAIN TECHNIQUES FOR ANALYZING PICOSECOND OPTICAL PULSES

12. PERSONAL AUTHOR(S)
John C. Swartz, Bob D. Guenther, Frank C. De Lucia

13a. TYPE OF REPORT	13b. TIME COVERED	14. DATE OF REPORT (Year, Month, Day)	15. PAGE COUNT
Final Report	FROM 5/10/88 TO 10/1/89	1990, February, 1	87

16. SUPPLEMENTARY NOTATION
The view, opinions and/or findings contained in this report are those of the author(s) and should not be construed as an official Department of the Army position, policy, or decision, unless so designated by other documentation.

17. COSATI CODES		
FIELD	GROUP	SUB-GROUP

18. SUBJECT TERMS (Continue on reverse if necessary and identify by block number)

19. ABSTRACT (Continue on reverse if necessary and identify by block number)

Using the techniques of Fourier analysis, any periodic time domain function will have a unique frequency domain transform. It is therefore possible to use frequency domain measurements to understand a time domain signal. Fourier analysis implies that picosecond laser pulses would have frequency components which range into the microwave bands.

The technique of picosecond demodulation is one way of generating microwaves from laser pulses. Picosecond demodulation uses laser pulsesto generate electron bunches at a photocathode. The electron bunches are then accelerated and radiate electromagnetic waves. Based on this technique it is possible to measure the microwave spectrum of a picosecond optical pulse train.

This report develops the theory of picosecond demodulation and shows that the frequency spectrum generated is related to the Fidrier transform of the time

20. DISTRIBUTION/AVAILABILITY OF ABSTRACT	21. ABSTRACT SECURITY CLASSIFICATION
☐ UNCLASSIFIED/UNLIMITED ☐ SAME AS RPT. ☐ DTIC USERS	Unclassified
22a. NAME OF RESPONSIBLE INDIVIDUAL	22b. TELEPHONE (Include Area Code) / 22c. OFFICE SYMBOL

DD FORM 1473, 84 MAR — 83 APR edition may be used until exhausted. All other editions are obsolete.

SECURITY CLASSIFICATION OF THIS PAGE
UNCLASSIFIED

90 03 06 045

(19) Continued,

domain envelope of the laser pulse train. Based on the theoretical development, a prototype device, called a picosecond demodulator, has been built. Using this device, several experiments are reported which (a) verify the theory of picosecond demodulation and (b) demonstrate that frequency domain techniques can be used to characterize picosecond pulses. These results indicate that frequency domain techniques are easy and inexpensive to implement and provide an accurate suplement to time domain measurements using autocorrelators or streak cameras.

FREQUENCY DOMAIN TECHNIQUES FOR ANALYZING PICOSECOND OPTICAL PULSES

Final Report

John C. Swartz
Bob D. Guenther
Frank C. De Lucia

February 1, 1990

U.S. Army Research Office

Contract DAAL03-88-C-0014

Duke University

UNCLASSIFIED
SECURITY CLASSIFICATION OF THIS PAGE

MASTER COPY - FOR REPRODUCTION PURPOSES

REPORT DOCUMENTATION PAGE

1a. REPORT SECURITY CLASSIFICATION Unclassified	1b. RESTRICTIVE MARKINGS
2a. SECURITY CLASSIFICATION AUTHORITY	3. DISTRIBUTION/AVAILABILITY OF REPORT Approved for public release; distribution unlimited.
2b. DECLASSIFICATION/DOWNGRADING SCHEDULE	
4. PERFORMING ORGANIZATION REPORT NUMBER(S)	5. MONITORING ORGANIZATION REPORT NUMBER(S)
6a. NAME OF PERFORMING ORGANIZATION Duke Univesity 6b. OFFICE SYMBOL (If applicable)	7a. NAME OF MONITORING ORGANIZATION U. S. Army Research Office
6c. ADDRESS (City, State, and ZIP Code) Durham, North Carolina, 27706	7b. ADDRESS (City, State, and ZIP Code) P. O. Box 12211 Research Triangle Park, NC 27709-2211
8a. NAME OF FUNDING/SPONSORING ORGANIZATION U. S. Army Research Office 8b. OFFICE SYMBOL (If applicable)	9. PROCUREMENT INSTRUMENT IDENTIFICATION NUMBER
8c. ADDRESS (City, State, and ZIP Code) P. O. Box 12211 Research Triangle Park, NC 27709-2211	10. SOURCE OF FUNDING NUMBERS PROGRAM ELEMENT NO. / PROJECT NO. / TASK NO. / WORK UNIT ACCESSION NO.

11. TITLE (Include Security Classification)
FREQUENCY DOMAIN TECHNIQUES FOR ANALYZING PICOSECOND OPTICAL PULSES

12. PERSONAL AUTHOR(S)
John C. Swartz, Bob D. Guenther, Frank C. De Lucia

13a. TYPE OF REPORT	13b. TIME COVERED	14. DATE OF REPORT (Year, Month, Day)	15. PAGE COUNT
Final Report	FROM 5/10/88 TO 10/1/89	1990, February, 1	87

16. SUPPLEMENTARY NOTATION
The view, opinions and/or findings contained in this report are those of the author(s) and should not be construed as an official Department of the Army position, policy, or decision, unless so designated by other documentation.

17. COSATI CODES		
FIELD	GROUP	SUB-GROUP

18. SUBJECT TERMS (Continue on reverse if necessary and identify by block number)

19. ABSTRACT (Continue on reverse if necessary and identify by block number)

Using the techniques of Fourier analysis, any periodic time domain function will have a unique frequency domain transform. It is therefore possible to use frequency domain measurements to understand a time domain signal. Fourier analysis implies that picosecond laser pulses would have frequency components which range into the microwave bands.

The technique of picosecond demodulation is one way of generating microwaves from laser pulses. Picosecond demodulation uses laser pulsesto generate electron bunches at a photocathode. The electron bunches are then accelerated and radiate electromagnetic waves. Based on this technique it is possible to measure the microwave spectrum of a picosecond optical pulse train.

This report develops the theory of picosecond demodulation and shows that the frequency spectrum generated is related to the Fidrier transform of the time

20. DISTRIBUTION/AVAILABILITY OF ABSTRACT ☐ UNCLASSIFIED/UNLIMITED ☐ SAME AS RPT. ☐ DTIC USERS	21. ABSTRACT SECURITY CLASSIFICATION Unclassified
22a. NAME OF RESPONSIBLE INDIVIDUAL	22b. TELEPHONE (Include Area Code) / 22c. OFFICE SYMBOL

DD FORM 1473, 84 MAR

83 APR edition may be used until exhausted.
All other editions are obsolete.

SECURITY CLASSIFICATION OF THIS PAGE
UNCLASSIFIED

(19) Continued,

domain envelope of the laser pulse train. Based on the theoretical development, a prototype device, called a picosecond demodulator, has been built. Using this device, several experiments are reported which (a) verify the theory of picosecond demodulation and (b) demonstrate that frequency domain techniques can be used to characterize picosecond pulses. These results indicate that frequency domain techniques are easy and inexpensive to implement and provide an accurate suplement to time domain measurements using autocorrelators or streak cameras.

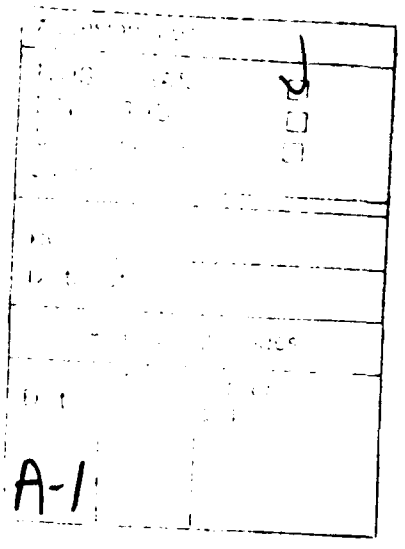

Abstract

Using the techniques of Fourier analysis, any periodic time domain function will have a unique frequency domain transform. It is therefore possible to use frequency domain measurements to understand a time domain signal. Fourier analysis implies that picosecond laser pulses would have frequency components which range into the microwave bands.

The technique of picosecond demodulation is one way of generating microwaves from laser pulses. Picosecond demodulation uses laser pulses to generate electron bunches at a photocathode. The electron bunches are then accelerated and radiate electromagnetic waves. Based on this technique it is possible to measure the microwave spectrum of a picosecond optical pulse train.

This paper develops the theory of picosecond demodulation and shows that the frequency spectrum generated is related to the Fourier transform of the time domain envelope of the laser pulse train. Based on the theoretical development, a prototype device, called a picosecond demodulator, has been built. Using this device, several experiments are reported which (a) verify the theory of picosecond demodulation and (b) demonstrate that frequency domain techniques can be used to characterize picosecond optical pulses. These results indicate that frequency domain techniques are easy and inexpensive to implement and provide an accurate supplement to time domain measurements using autocorrelators or streak cameras.

Acknowledgements

This thesis would not have been possible without the help and support of many people. I would like to thank my supervisor, Dr. Bob Guenther whose enthusiasm, encouragement, and insight have been my greatest inspiration. I must also thank Dr. Frank De Lucia for his constant advice and support. This project owes much of its success to their collaboration.

Special thanks also goes to the US Army Research Office for sponsoring this research under contract DAAL03-88-C-0014 and to Dr. Craig Casey for overseeing this project through the Duke Department of Electrical Engineering. Without their sponsorship and oversight none of this work would have been possible.

Thanks also goes to Dr. John Thomas and his group for sharing with me both their lab space and their insight into lasers. Also, I would like to thank Dick Poole for his assistance in the Machine Shop. For all the help finding research material, I am also grateful to Eric Smith, in the Engineering Library, and Bonnie Springer and Judy Boone, in the Physics Library.

Finally, and most importantly, I would like to thank my wife Kim and my parents for putting up with my erratic schedule, my piles of notes and stuff, and my occasional disorganization. I do not know where I would be without their love and support .

Contents

List of Illustrations

List of Tables

Glossary

a^* .....complex conjugate of a

c.c.....complex conjugate of previous term

$F(t)$....a time domain function, F

$G(\omega)$..a frequency domain function, G

$\otimes$ .....convolution operator defined as, $g(t) \otimes h(t) \equiv \int_{t=-\infty}^{\infty} g(t)h^*(\tau - t)dt$

$\oplus$ .....correlation operator defined as, $g(t) \oplus h(t) \equiv \int_{t=-\infty}^{\infty} g(t)h^*(t - \tau)dt$

$*$ .....arithmetic multiplication operator (not to be confused with $\otimes$ or $\oplus$).

FT.....Fourier transform operator, $\mathsf{FT}\{f(t)\} \equiv F(\omega) \equiv \int_{t=-\infty}^{\infty} f(t)e^{-i\omega t}dt$

Chapter 1

Background

1.1 Introduction

During the past decade, the study of short time phenomena has accelerated due to the development of ultrashort pulsed lasers and ultrashort measurement techniques. Femtosecond lasers are now commonly used to study chemical, biological, and electrical phenomena, while measurement devices such as streak cameras and autocorrelators are capable of measuring with picosecond and femtosecond resolution, respectively. These measurement devices work entirely in the time domain. However, based on the principles of Fourier Analysis, the same amount of information is available from measurements made in the frequency domain. A typical example is shown in fig. 1-1; a square wave in the time domain is equivalent to a sinc function in the frequency domain. Depending on the phenomena of interest, either representation of the signal may be used to study a system.

This thesis describes the theory and implementation of frequency domain instrumentation for analyzing short time domain phenomena, specifically measuring the output characteristics of picosecond optical pulses. This chapter provides background material for this research. First, the current technology of generating ultrashort laser pulses is reviewed. Next, time domain methods for analyzing picosecond laser pulses are discussed. Finally, the various techniques of generating microwave (frequency domain) spectra from short time laser pulses is reviewed and shown to be the foundation for frequency domain analysis methods.

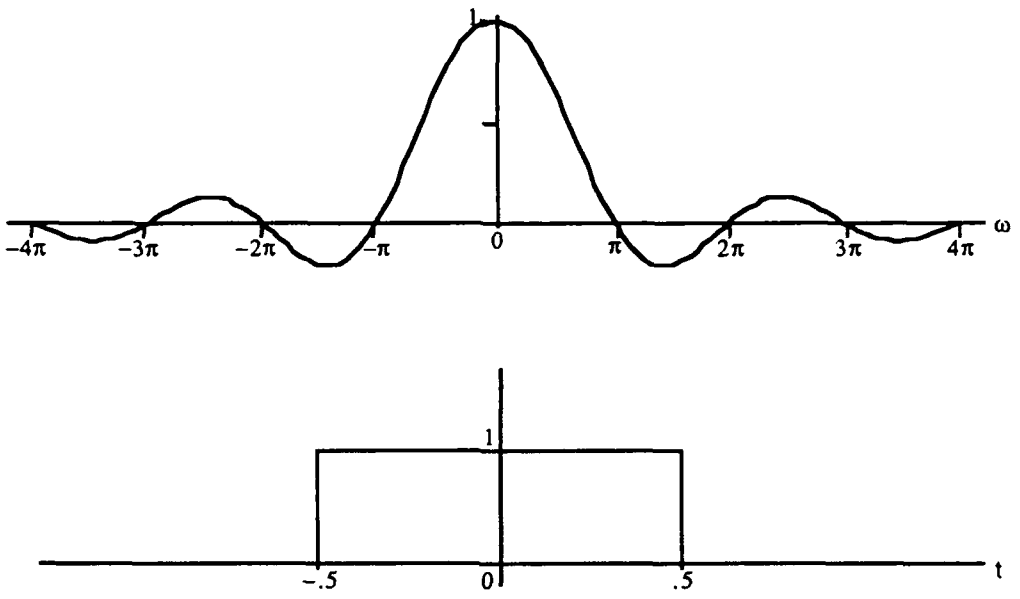

Fig. 1-1. The rect(t) functi : and its Fourier transform sinc(ω)

1.2 Generation of Picosecond Laser Pulses

The first picosecond pulsed laser was reported by DeMaria et al. in 1966 [1]. During the past twenty years much work has been done developing systems that produce shorter and shorter width pulses [2]. Currently, the shortest pulses produced are 6 fs long [3]. In the laboratory, ultrashort laser pulses are generated using one of three common systems: synchronously pumped dye lasers, colliding pulse mode locked lases, or laser pulse compressors.

1.2.1 Synchronously Pumped Dye Lasers

A typical synchronously pumped dye laser is shown schematically in fig. 1-2. The pump laser is mode locked to produce a periodic train of short pulses. These pulses are typically a fraction of a nanosecond long and pump the gain medium in the dye laser cavity. The time spacing between pulses equals the round trip transit time of a single pulse in the laser cavity; for a cavity of length l, the period between pulses $T=c/2l$ where c is the speed of light in the cavity.

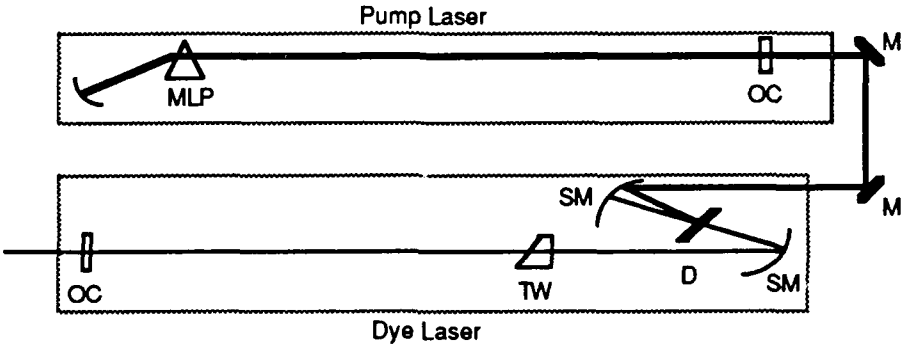

Fig. 1-2. Schematic of a synchronously pumped dye laser: MLP, mode lock prism; OC, output coupler; M, flat mirror; SM, spherical mirror; D, dye jet; TW, tuning wedge.

In steady state, a single short optical pulse travels through the dye laser cavity. When the dye and pump laser cavity lengths are properly aligned, the pulse in the dye cavity has the same period as the pump laser pulse, but reaches the gain media slightly after the pump pulse. The pump pulse excites the dye molecules, creating population

inversion. Immediately following inversion, the dye cavity pulse hits the excited dye molecules and causes stimulated emission, hence producing laser action. Because the stimulated emission lifetime is extremely short, the dye cavity pulse is shorter than the pump pulse duration. It is in this way that a relatively long (typically nanosecond) pump pulse can produce a much shorter (≈a few picoseconds) dye laser pulse.

Although not "state of the art", synchronously pumped dye lasers are widely used because of several useful characteristics. First, these lasers are uncomplicated to build and easy to maintain. Second, the output wavelength of the laser is selected with an etalon or optical wedge inside the dye laser cavity. As a result, the output spectral width of the dye laser is narrow and can be tuned across the spectrum supported by the dye gain curve. The work presented in this paper used a synchronously pumped dye laser system.

1.2.2 Colliding Pulse Mode Locked Lasers

Colliding pulse mode locked (CPM) lasers [4] can produce sub-picosecond pulses; simple CPM lasers easily generate 200 femtosecond pulses. Shown in fig. 1-3, the topology of the CPM laser is different than that of the synchronously pumped dye laser. Using a ring topology, the CPM laser is a passively mode locked system, with two counterpropagating pulses. When the dye and absorber jets are separated by a quarter of the ring length, the laser supports two counterpropagating pulses such that the pulses collide at the absorber jet (A, in fig. 1-3) and are a half ring distant when either hits the dye jet (D in fig. 1-3).

Although a relatively new device, several useful characteristics have made the CPM laser a preferred instrument in ultrashort time research. With dispersion compensation (the shaded path and prisms shown in fig. 1-3) produce pulses as short as 27

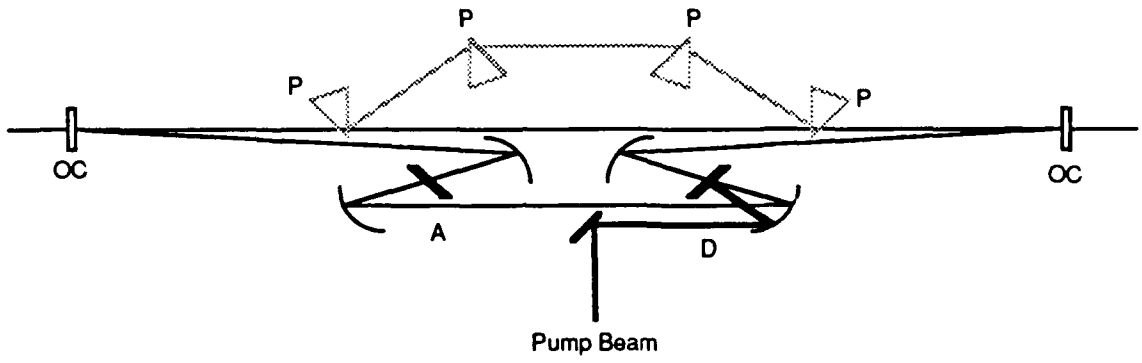

Fig. 1-3. Schematic of colliding pulse mode locked laser: A, saturable absorber; D, dye jet ; OC, output coupler; P, prism. The shaded figures indicate the optical path for dispersion compensation. With compensation, this design produces 27 femtosecond optical pulses.

femtoseconds [5]. Even without compensation, 150 femtosecond pulses are normally generated. With appropriate dye and absorber combinations, the output wavelength may be tuned across the entire optical spectrum [6]. Finally, because the CPM laser uses a c.w. pumping source (unlike the synchronously pumped dye laser) the overall cost and complexity of this system is relatively low.

1.2.3 Laser Pulse Compression

The generation of minimum length optical pulses requires the use of an external pulse compressor. Optical pulse compressors have their origins in microwave pulse compressors built in the 1950's [7]. Optical pulses are compressed in two steps. First the optical pulse is stretched in time and chirped in frequency (fig. 1-4); this is done by propagating a high energy pulse through a optical fiber (self phase modulation results in

positive linear dispersion and a lengthening of the pulse). The chirped pulse is compressed by transit through a pair of gratings or prisms. The grating pair produces linear dispersion without changing the time width of the pulse's intensity envelope. When properly aligned, the dispersion of the grating pair can be made to cancel the dispersion caused by the fiber. This results in all the spectral components of the optical pulse overlapping with no phase difference; in the time domain, this yields pulses much narrower than the original pulse.

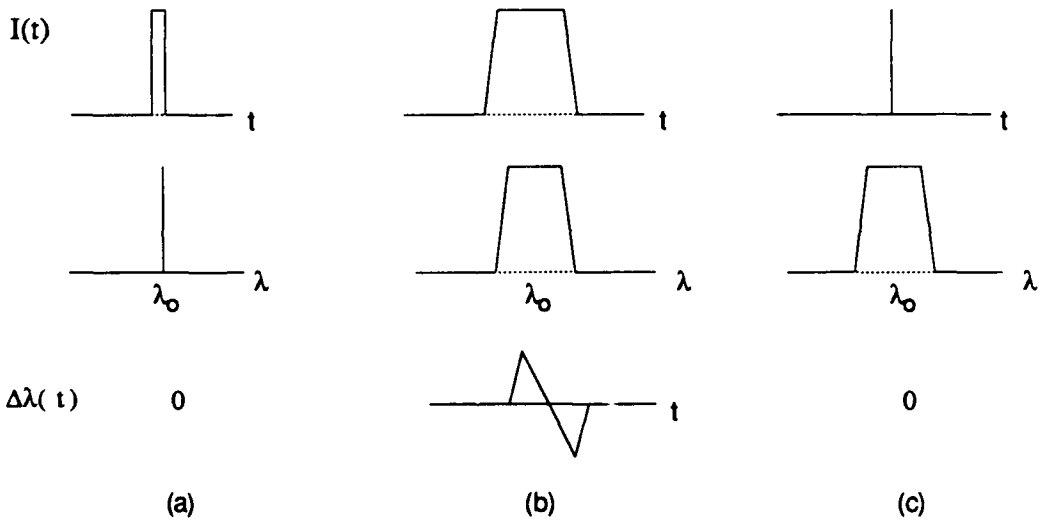

Fig. 1-4. Optical pulse compression. The top row is the time envelope of the pulse. The second row shows the optical wavelength spectrum of the pulse. The bottom row indicates the change of wavelength versus time (chirp). (a) is the shows the pulse characteristics before chirping, (b) shows the chirped pulse, (c) depicts the pulse after compression.

1.3 Measurement of picosecond pulses in time

In conjunction with the development of picosecond laser sources there has been a corresponding development of instruments capable of measuring optical phenomena of short time duration. Although a wide variety of devices have been devised, two classes of measurement devices are typically used to measure short time phenomena: streak cameras and autocorrelators.

1.3.1 Streak Cameras

A simple streak camera is shown in fig. 1-5. In operation, a short optical pulse hits the photocathode and simultaneously triggers the electrode sweep voltage. The time profile of the electron density corresponds to the optical intensity time profile. As the photoelectrons travel from the photocathode to the anode, the time varying electrode

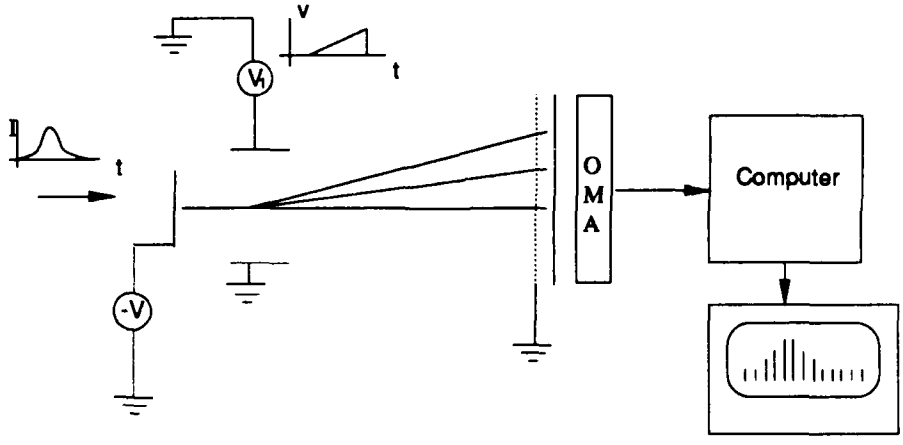

Fig. 1-5. Schematic of a simple streak camera: $\underline{V_1}$, sweep generator; $\underline{V}$, photocathode supply; $\underline{P}$, photocathode; $\underline{OMA}$, optical multichannel analyzer.

potential V_1 will produce a time varying force, deflecting the electron beam. Electrons generated early in the sample time will hit near the bottom of the display anode, while electrons generated later will strike the anode higher. The electron density, proportional to the input optical beam intensity, generates light when it strikes the phosphor on the anode. The phosphor display will produce an intensity proportional to the time intensity of the input beam.

Current state-of-the-art streak cameras have a limiting time resolution form 0.7 picoseconds [8] to 0.5 picoseconds [9]. Baggs et al. [8] state that the limiting resolution of 0.2 picoseconds is potentially realizable. Streak cameras have also been built to collect multiple channels of data simultaneously [10]. An early demonstration of this technique by Seymour and Alfano [11] simultaneously measured the left and right circular polarization profile of semiconductor lasers.

Although quite useful, the use of streak cameras is limited for two reasons. First, streak cameras (and the associated drive and analysis electronics) are quite expensive. Second, streak cameras are also limited by the dynamic range and spectral sensitivity of the phototube; operation at infrared requires a different phototube than operation in the visible [12].

1.3.2 Autocorrelators

The second widely used method of short time measurement is autocorrelation. The autocorrelator produces an output modelled by,

$$A(\tau) = \int f(t)f(t-\tau)dt \qquad (1.1)$$

$$= f(t) \oplus f(t)$$

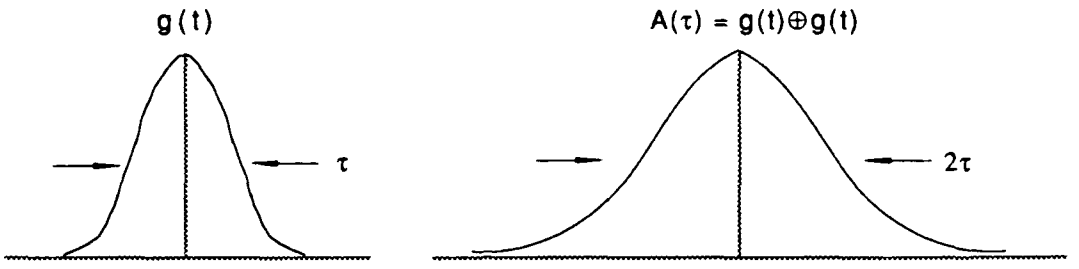

Fig. 1-6. Autocorrelation of a gaussian shaped pulse.

where $f(t)$ is the optical input intensity, τ is the optical delay, and $A(\tau)$ is the autocorrelation ($\oplus$ denotes the correlation operator). It is important to note that the integrand of equation (1.1) is dependent on the initial pulse shape. Hence, the autocorrelator generates a non-linear measurement of the pulse width. The autocorrelation for a gaussian pulse is shown in fig. 1-6.

A variety of optical phenomena have been used to build autocorrelators, including phase conjugation [13], two-photon flourescence [14], and second harmonic generation (SHG). Of these, the typical hardware implementation uses SHG and a Michelson interferometer (fig. 1-7). The input optical beam is split, and half of the beam is delayed by the variable length arm, l. The two beam components are slightly offset (by the roof-top prisms) and focused through the SH media. When photons coincide in time and space in the SH media, frequency doubling occurs and a photon of 2ω is generated. The intensity of the doubled photons correspond to the integral of equation (1.1), where τ is

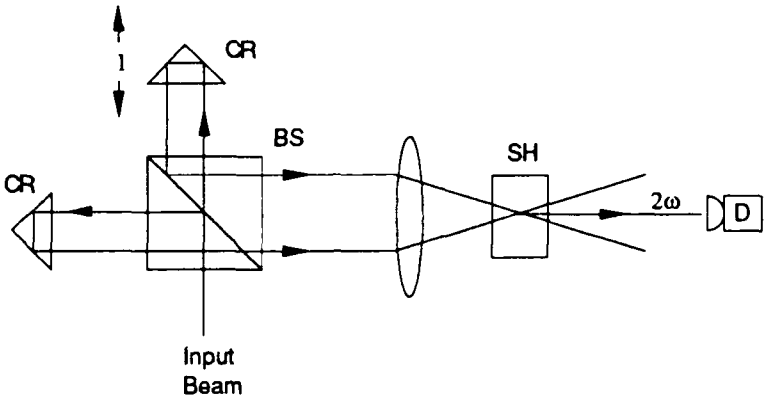

Fig. 1-7. Autocorrelator schematic: CR, corner reflector; BS, beam splitter; SH, second harmonic crystal; D, detector; l, optical delay path.

the delay imposed by the variable arm ($\tau=l/c$). The readout electronics measure the detector response as the delay arm length varies and displays the result.

Autocorrelators have been built around several designs. Commercial models are available but are quite expensive. Due to limits imposed by the SH media available, autocorrelation is limited to visible and infrared light. Also, because autocorrelators are multi-element optical devices, they require careful alignment and periodic maintenance. The problem of alignment is most severe when aligning a wavelength tunable dye laser. In this situation, changes of either the laser optics or the operating wavelength require realignment of the autocorrelator. Finally, in practice the autocorrelation function requires an *a priori* knowledge of the pulse shape to accurately determine its width; conversion factors for several shapes are shown in table 1.

Table 1. Comparison of full width at half maximum of a function and its autocorrelation.; t_{FW} is the full width at half maximum of the original function and τ_{FW} is the full width at half maximum of the autocorrelation of the function. The values for $sech^2$ were obtained in closed form, based on results given by Yariv [42].

f(t)	t_{FW} = FWHM{f(t)}	τ_{FW} = FWHM{f(t)⊕f(t)}	τ_{FW}/t_{FW}
$\exp(-t^2/a^2)$	$2a\sqrt{\ln 2}$	$2a\sqrt{2}\sqrt{\ln 2}$	$\sqrt{2}$
rect(t/a)	a	a	1
$\exp(-t/a)$, $t\geq 0$	$a\ln 2$	$2a\ln 2$	2
$sech^2(t/a)$	$a\ \mathrm{arccosh}(\sqrt{2})$	$2a[\mathrm{arccosh}(\sqrt{2})]^3$	$2[\mathrm{arccosh}(\sqrt{2})]^2$

1.4 Generation of frequency domain information from picosecond pulses

The conversion of picosecond optical pulses to their frequency domain components is based on techniques by which microwaves may be generated from optical pulses. The earliest uses of lasers to generate microwave radio waves used klystrons and traveling-wave tubes (TWTs) in which the buncher elements were replaced by a photocathode. A pulsed laser would drive the cathode producing beams of bunched electron capable of driving the microwave structures at resonance. Proposed in 1955 [15] and 1960 [16], this approach was first realized by McMurty and Siegman in 1961 [17]. By focusing a laser on the cathode of a TWT, McMurty and Siegman amplified the beats produced by the axial modes of a ruby laser; microwave signals were generated from 1.8 GHz to 4.2 GHz at 600 MHz intervals. Various later experiments used modified TWTs [18],

klystrons [19], and modified phototubes [20] to produce X-band (8-12 GHz) microwaves.

By the mid 1960's researchers began using semiconductor photodiodes to replace the vacuum tube devices [21]. During the 1970's, research concentrated on switching of microwave signals by optical control; several groups developed electro-optical devices for modulating microwave signals propagating through semiconductor transmission lines [22, 23]. Mourou, Stancampiano, and Blumenthal [24] reported the first solid state system for generating microwaves from picosecond optical pulses. Shown in fig. 1-8, their system used a fast GaAs photodiode to switch a high voltage across an X-band waveguide; the system produced 50 pS microwave pulses which were used in a simple radar demonstration.

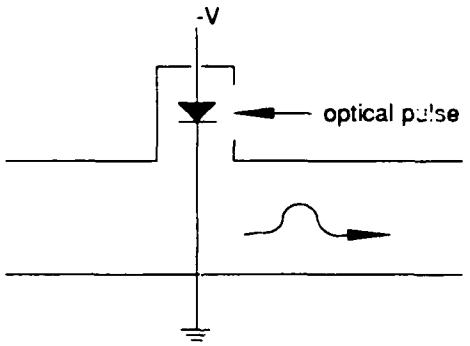

Fig. 1-8. A solid state device for generating microwaves.

In the early 1980's, an approach was developed for generating microwaves by direct demodulation of picosecond optical pulses. First described by De Lucia [25] and

De Lucia, Guenther, and Anderson [26], the technique of picosecond demodulation uses a simple vacuum tube photodiode to remove the carrier from an optical pulse, leaving the envelope spectrum centered at DC. (Picosecond demodulation is analogous to the operation of an AM crystal radio receiver.) Within the past two years, several researchers [28, 29, 30] have used solid-state variations of this technique to generate microwave radiation of terahertz frequencies (wavelengths of less than .3 mm). Most recently this technique has been used to generate microwaves for measuring complex dielectric constants [27]. Grischkowsky has suggested that terahertz microwave sources may also be useful for transmission spectroscopy and high speed communications [29].

1.5 Optical pulse analysis by picosecond demodulation

This thesis uses the technique of picosecond demodulation to determine the pulse width of a picosecond optical pulse. Demonstrated in the next chapter, the microwave radiation spectrum produced by the picosecond demodulator is related to the Fourier transform of the time domain laser pulse envelope. Based on simple measurements of the microwave spectrum (e.g., rolloff), the optical pulse width may be determined. Although this may seem like an indirect measurement approach, this paper will demonstrate that frequency domain information is as useful as that of the time domain and the basic frequency domain techniques are simpler to implement than time domain instruments.

In the next chapter the theory of picosecond demodulation is presented along with its application to the model of a picosecond pulsed laser system. The third chapter describes the actual experimental setup and presents the data obtained. The final chapter discusses the results and compares them to theoretical expectations.

Chapter 2

Theory

2.1 Overview

This chapter presents the theory of operation of the picosecond demodulator. This chapter is divided into three sections. The first section develops the frequency domain model of picosecond optical pulses. The second section describes the microwave and photoemission theory required to describe the operation of the picosecond demodulator. The last section brings the previous sections together and describes various methods of determining time domain pulse parameters from the frequency domain data.

2.2 Laser Pulse Theory

The most common approach of analyzing picosecond pulses is based on the analysis of laser mode locking. In addition to yielding a good description of picosecond pulses in both the time and frequency domain, this approach gives good insight into the way lasers actually produce a pulsed output. An alternate method of analyzing picosecond pulses uses systems theory. This approach is appealing because it is builds on techniques of system analysis taught in most undergraduate electrical engineering curricula [33]. Both approaches are developed in this section.

2.2.1 Mode Locking Analysis of Laser Pulse Trains

The theory of laser mode locking provides a description and model of picosecond lasers pulses [25,32]. The laser produces a train of pulses of width τ and period T (fig. 2-1).

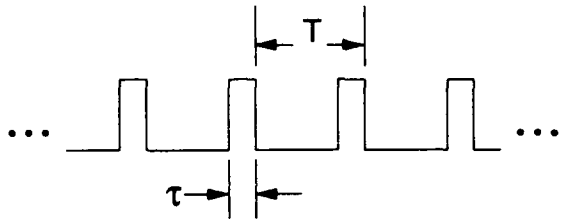

Fig. 2-1. Pulse Train produced by mode locked laser.

The total electric field of the laser output can be expressed as Fourier series, with the individual terms correspond to the longitudinal modes supported by the laser cavity,

$$\begin{aligned} E_T(z,t) &= \frac{E_o}{2} + \tfrac{1}{2}\sum_{k=1}^{\infty} E_k e^{i(\omega_k[t-z/c]+\phi_k)} + \tfrac{1}{2}\sum_{k=1}^{\infty} E_k e^{-i(\omega_k[t-z/c]+\phi_k)} \\ &= \frac{E_o}{2} + \tfrac{1}{2}\sum_{k=1}^{\infty} E_k e^{i(\omega_k[t-z/c]+\phi_k)} + \text{c.c.} \end{aligned} \tag{2.1}$$

where ϕ_k and E_k are the phase and magnitude of the kth harmonic mode. The laser cavity, however, does not support all these modes. Instead, only a finite number of modes are supported. Assuming the laser supports N modes, a change of indices allows equation (2.1) to be rewritten as,

$$E_T(z,t) = \tfrac{1}{2}\sum_{n=-\frac{N-1}{2}}^{\frac{N-1}{2}} E_n e^{i(\omega_n[t-z/c]+\phi_n)} + \text{c.c.} \tag{2.2}$$

where it is assumed that N is odd. The frequency of the nth mode is defined as,

$$\omega_n = \omega_0 + n\Delta \tag{2.3}$$

where ω_0 is the center laser frequency and $\Delta=2\pi(c/2l)$ is the laser cavity longitudinal mode spacing in angular frequency.

Observing the pulse at an arbitrary point z=0 and rearranging the terms in (2.2) yields[1],

$$\begin{aligned} E_T(0,t) &= \tfrac{1}{2}e^{i\omega_o t}\sum_n E_n e^{i(n\Delta t+\phi_n)} + \tfrac{1}{2}e^{-i\omega_o t}\sum_n E_n e^{-i(n\Delta t+\phi_n)} \\ &= \cos(\omega_o t)\sum_{n=-\frac{N-1}{2}}^{\frac{N-1}{2}} E_n \cos(n\Delta t+\phi_n) \end{aligned} \tag{2.4}$$

The the cosine term in ω_0 represents the optical carrier at the center frequency of the laser. The summation represents the optical pulse envelope whose shape is dependent on E_n and ϕ_n.

If no other control is placed on the laser cavity, all the modes will oscillate with independent phase and amplitude (ignoring mode competition effects [pp. 992-1002, reference 4]). However, by controlling the phase of each mode it is possible to control the laser output. Forcing ϕ_n equal to a constant, ϕ_0, allows the phase term within the summation of eq. (2.4) to be treated as a multiplicative phase constant,

$$E_T(0,t) = \cos(\omega_o t+\phi_o)\sum_{n=-\frac{N-1}{2}}^{\frac{N-1}{2}} E_n \cos(n\Delta t) \tag{2.5}$$

In this case, all the modes oscillate in unison, and the laser is said to be mode-locked. A

---

[1] For any complex X, $X+X^*=2\mathrm{Re}\{X\}$.

further simplification can be made by assuming $\phi_0=0$. When the goal of the analysis is an understanding of the laser intensity envelope, this assumption is always valid.

Assuming the mode locked laser cavity supports N modes all with $\phi_n=0$, and assuming that gain saturation forces[2] $E_n = E_0$ for all n (this will be relaxed in the next section), equation (2.5) further reduces to,

$$E_T(0,t) = E_o \cos(\omega_o t) \sum_{n=-\frac{N-1}{2}}^{\frac{N-1}{2}} \cos(n\Delta t) \tag{2.6}$$

$$= \cos(\omega_o t) \frac{\sin(N\Delta t/2)}{\sin(\Delta t/2)} \tag{2.7}$$

and hence the laser output intensity is,

$$I \propto |E|^2$$

$$I \propto \frac{\sin^2(N\Delta t/2)}{\sin^2(\Delta t/2)} \tag{2.8}$$

Equation (2.8) is periodic (with period $T=2\pi/\Delta=2l/c$) therefore the mode-locked laser output is a train of pulses. The individual pulses have a peak power N times the average power and a width proportional to $c/2lN$. If the spatial variation of the field is reinserted, equation (2.8) becomes,

$$I \propto \frac{\sin^2\{N\Delta(t-z/c)/2\}}{\sin^2\{\Delta(t-z/c)/2\}} \tag{2.9}$$

indicating that within the cavity a single short pulse bounces between the cavity mirrors.

---

[2] This is generally valid for mode locked lasers.

Physically, the individual modes may be synchronized by modulating the optical beam (e.g., gain modulation, acousto-optical shutter, etc.). As shown in fig. 2-2, amplitude modulation of the optical field produces sidebands on either side of the cavity modes. When the modulation frequency equals the mode spacing frequency, the sidebands from one mode will overlap with the fundamental of adjacent modes (fig. 2-2b). The sidebands of one longitudinal mode couple with the adjacent fundamentals forcing the sidebands to have the same phase as the neighboring fundamental. Because the sidebands of a given fundamental differ only in frequency and not in phase, the overlapping of sidebands with adjacent fundamentals force all modes to oscillate with identical phase, hence, producing mode locking.

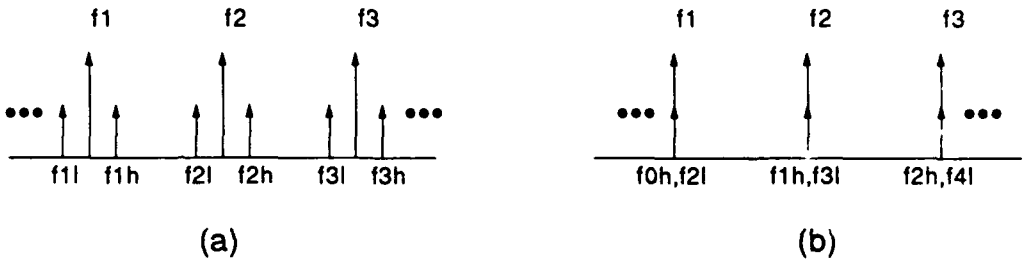

Fig. 2-2. Laser mode locking by sideband coupling. The fundamentals are labeled f1,f2,f3,... The first lower and upper harmonics are denoted by the l and h suffixes. a) shows the primary sidebands when the mode lock frequency is less than the mode spacing frequency. b) shows the primary sidebands from adjacent modes overlapping the fundamentals.

2.2.2 Systems Theory Analysis of Laser Pulse Trains

The previous section assumed $E_n=E_o$ for all n. Although this assumption is usually valid for mode locked lasers, using a systems approach yields an analysis which better accommodates laser pulses with generalized longitudinal mode spectrum (as shown in fig. 2-3).

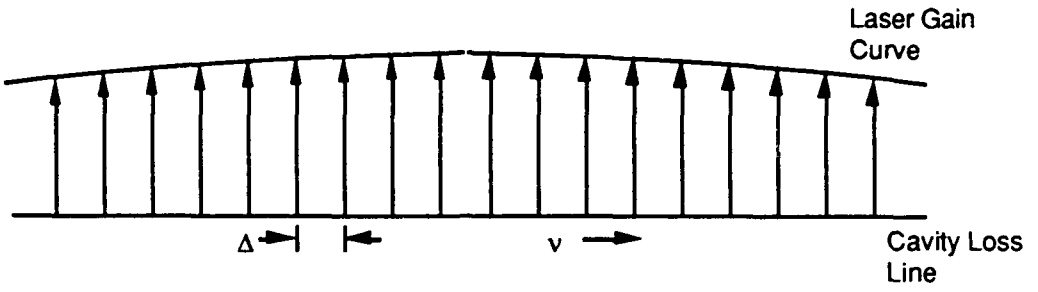

Fig. 2-3. Generalized laser gain curve. The cavity longitudinal mode spacing is Δ.

In the frequency domain the complete laser field is described by,

$$E_L(\omega) = comb_\Delta\left\{\tfrac{1}{2}\left[\delta(\omega-\omega_o)+\delta(\omega+\omega_o)\right]\otimes G(\omega)\right\} \tag{2.10}$$

$$E_L(\omega) = \tfrac{1}{2}comb_\Delta\left\{G(\omega-\omega_o)+G(\omega+\omega_o)\right\} \tag{2.11}$$

where $\otimes$ is the convolution operator, $G(\omega)$ is the laser gain curve function, Δ is the longitudinal mode spacing, and ω_0 is the optical angular frequency at the center (with

respect to the cavity loss line intercepts) of the gain curve function[3].

The time response of the laser is found by taking the Fourier transform of equation (2.11),

$$\begin{aligned} E_L(t) &= \mathrm{FT}\{E_L(\omega)\} \\ &= T\,\mathrm{rep}_T\left\{\cos(\omega_o t) * g(t)\right\} \end{aligned} \tag{2.12}$$

where T, the pulse period, is defined as $1/\Delta$ and $g(t)$ is the Fourier transform of the gain curve and yields the time domain pulse shape (assuming a reference point in space at z=0). Equation (2.12) shows that in the time domain the output of a pulsed picosecond laser can be modelled as an optical carrier modulated by a periodic envelope (fig. 2-4).

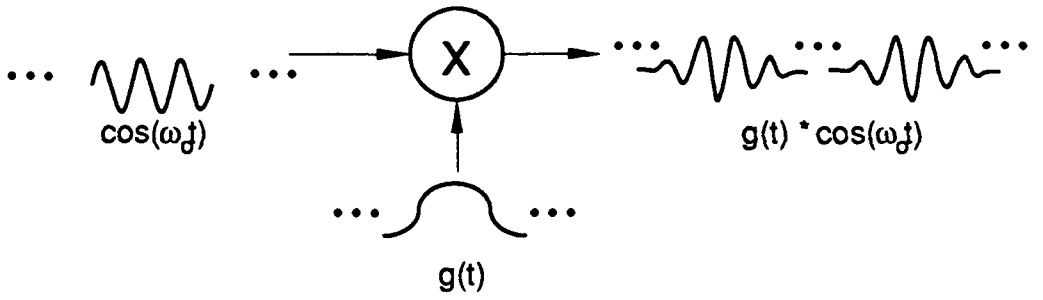

Fig. 2-4. Pulse formed by envelope modulating an optical carrier. $\mathrm{Cos}(\omega_0 t)$ is the optical carrier, g(t) is the periodic envelope function. The output is the product of the two functions.

---

[3] Note the following definitions:

$$\mathrm{rep}_T\{f(t)\} \equiv f(t) \otimes \sum_{n=-\infty}^{\infty} \delta(t - nT) \qquad \mathrm{comb}_T\{f(t)\} \equiv f(t) * \sum_{n=-\infty}^{\infty} \delta(t - nT)$$

It can be shown that the Fourier transform of these are,

$$\mathrm{comb}_T\{f(t)\} \Leftrightarrow \tfrac{1}{T}\,\mathrm{rep}_{1/T}\{F(\omega)\} \qquad \mathrm{rep}_T\{f(t)\} \Leftrightarrow \tfrac{1}{T}\,\mathrm{comb}_{1/T}\{F(\omega)\}$$

The previous section assumed $E_n=E_o$ for all N modes; using the systems approach this is equivalent to using equation (2.11) with[4],

$$G(\omega)=\text{rect}(\omega/N\Delta)$$

The complete time domain wave is[5],

$$\begin{aligned} E_L(t) &= \tfrac{1}{\Delta}\text{rep}_{1/\Delta}\left\{\cos(\omega_o t)\frac{\sin(N\Delta t/2)}{t/2}\right\} \\ &= \text{rep}_{1/\Delta}\left\{\cos(\omega_o t)\frac{\sin(N\Delta t/2)}{\Delta t/2}\right\} \end{aligned} \tag{2.13}$$

where $T=1/\Delta$ has been freely substituted. From this result, the envelope function of an individual pulse is,

$$g(t) = \frac{\sin(N\Delta t/2)}{\Delta t/2} \tag{2.14}$$

This result appears to be in conflict with equation (2.7). However, note that the $\text{rep}_{1/\Delta}\{\}$ operator produces an infinite sum of the argument function spaced $1/\Delta$. When the argument has infinite range, as does $g(t)$ in equation (2.14), then the periodically spaced functions overlap and add. Analyzed graphically, it can be shown that when N is large, equations (2.7) and (2.14) are equivalent. This is demonstrated in fig. 2-5 for N=11 and where the first three terms of the $\text{rep}_T\{\}$ summation are used.

---

[4] rect(ω) is defined as 1 on the interval [-ω/2,ω/2], and 0 elsewhere.

[5] Note that the Fourier transform of F(ω)=rect(ω/a) is f(t)=sin(at/2)/(t/2).

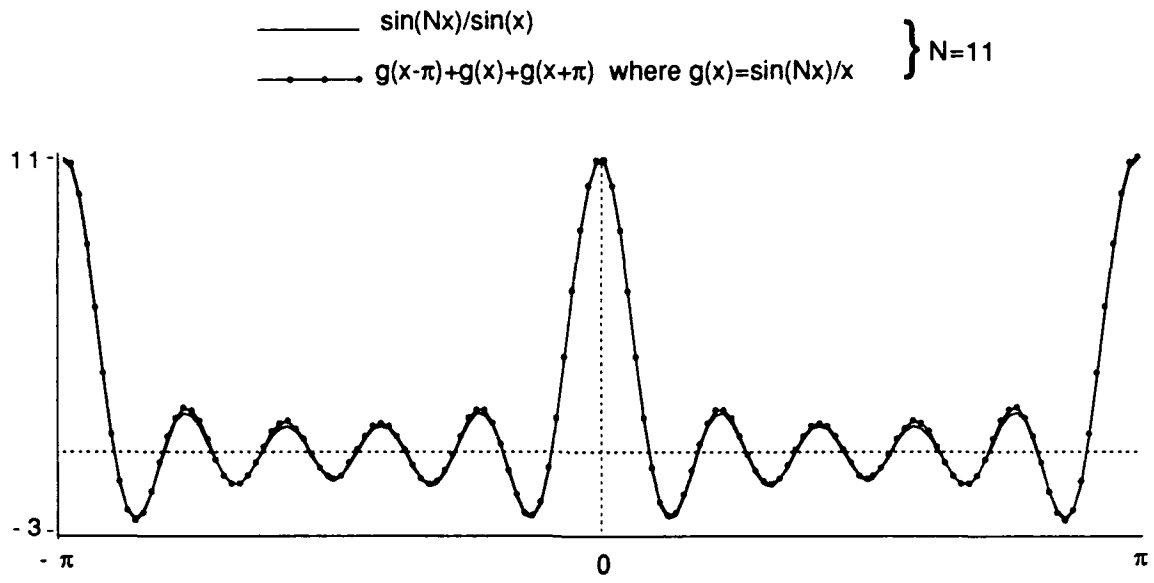

Fig. 2-5. Equations (2.7) and (2.14) compared for N=11.

The intensity of the field from equation (2.14) is generally difficult to solve in closed form. However, if the period, $T=1/\Delta$, between pulses is much larger than the rolloff of the envelope function, $g(t)$, then the envelope of the individual pulses is approximated by a single term of the rep{ } summation, i.e.,

$$\lim_{t \to \text{large}} \{g(t)\} \to 0$$

$$\therefore \lim_{\substack{T \to \text{large}, \\ t \ll T}} \{rep_T(g(t))\} \to g(t)$$

This is generally the case for picosecond pulsed lasers. Therefore, in this limit the intensity envelope of a single pulse is simply,

$$I \propto g^2(t)$$

The systems approach has two advantages. First, it does not impose any restrictions on the number of modes supported by the laser, i.e., N may be odd or even. This also relaxes the restriction of the previous section that ω_0 rest on a supported cavity mode. Second, the system approach allows a simple approach to handling laser pulses when $E_n \neq E_o$. As will be shown below, this approach clearly relates the time domain pulse shape to the frequency domain components, and therefore the output of the picosecond demodulator. See appendix A for further examples.

2.3 Picosecond Demodulator Operational Theory

The picosecond demodulator converts the time domain intensity profile of an optical pulse to its corresponding frequency domain spectrum. The picosecond demodulator performs the conversion in two steps. First, the optical pulse is used to produce an density modulated electron beam whose density profile in time is related to the intensity profile in time of the optical pulse. The electron bunch is then accelerated to produce a microwave field whose spectrum is related to the optical pulse profile and the picosecond demodulator cavity geometry. The following sections present the detailed theory of these operations.

2.3.1 Conversion of optical pulses to electron bunches

The picosecond demodulator uses a simple vacuum photodiode to convert the optical pulses to electron bunches. Based on the principles of photoemission, the number of electrons emitted by the photocathode is directly proportional to the intensity of the incident light [34,35],

$$\rho(t) \propto I(t) = |E(t)|^2 \tag{2.15}$$

where $\rho(t)$ is the charge density, $I(t)$ is the optical intensity, and $E(t)$ is the incident field. If the light intensity is a time dependent function, then the number of electrons produced will have the same time dependence.

The potential difference between the cathode and anode accelerates the photoelectrons across the gap between the electrodes. At any position in this gap the electron density will have the same time dependence as the optical pulses. As discussed in the previous section, the optical pulses may be modelled as a sum of sinusodal components. Therefore in operation the phototube can be thought of supporting a stream of electrons whose density in time is the sum of many currents each with sinusodal time dependence of varying frequency.

During the generation and transit of the electron bunches, two phenomena must be considered: photoemission response time and space charge spreading. (Other effects due to work function variations are considered in Appendix C.)

Very little information exists about the speed of the photoemission process. Spicer and Wooten [36] indicates that the rate is dependent on the penetration depth of the

radiation. Although no exact parameters are given, Spicer and Wooten indicate for metals, with shallow penetration depths, the response time will be on the order of 10 femtoseconds. Recent literature on the development of streak cameras implies that the photoemission process is much faster than 100 femtoseconds [37]. Compared to the duration of the picosecond optical pulses used in this paper, photoelectron emission can be considered instantaneous.

When a number of like charged particles are bunched together, Coulombic forces are generated which will force the particles to separate. In the analysis of klystrons, this effect is called space charge debunching [41]. The electron bunches generated in the phototube are essentially the same as the bunches found in a klystron, therefore, space charge debunching in the picosecond demodulator may be analyzed using the results of klystron theory. In the work described here, the electron bunch charge densities are small (approximately 10^{-12} Coulombs) and the transit times are quite short (typically <300 pS). Operating in this regime, klystron theory yields accurate results by assuming the electrons do not interact and are simply ballistic. Based on this assumption, the electron bunches generated in the phototube are assumed to maintain a spatial profile identical to the temporal laser pulse profile. (Appendix D presents a calculation that supports this result.)

2.3.2 Coupling of electron energy to the microwave field

In the picosecond demodulator, energy obtained from the constant accelerating field (between the phototube electrodes) is transferred from the electron beam to the microwave field in the waveguide. This section relates the frequency spectrum of the waveguide microwave field to the time profile of the electron bunch and hence the optical pulse shape.

In the picosecond demodulator the transfer of energy from the electron bunches to the microwave field is similar to the energy transfer that occurs in the catcher element of a klystron tube [38,39]. A density modulated electron beam passes a gap in a microwave structure, causing energy to transfer from the electron beam to the microwaves. The basic operation of the klystron is explained in terms of basic field theory and conservation of energy. Based on the analysis by De Lucia [25], a similar approach is used to explain the operation of the picosecond demodulator.

The basic waveguide setup is shown in fig. 2-6. When an electron leaves the surface of the photocathode, the DC potential causes the electron to accelerate to the

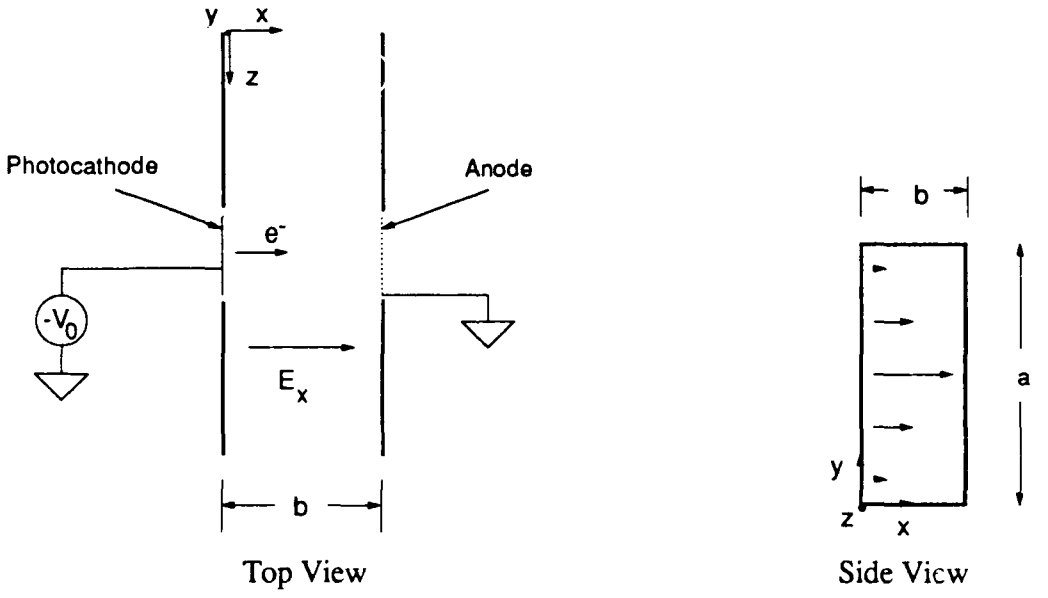

Fig. 2-6. Picosecond Demodulator Waveguide and Photodiode. Note that E_x is the microwave field supported by the waveguide; the electron is accelerated by the field $-V_o/b\,\hat{x}$.

anode. The motion of the electron can be determined by solving the equation of motion,

$$F = \frac{d(mv)}{dt} = \frac{V_0}{b} q$$

where m is the electron rest mass, q is the electron charge (q is a positive value equal $1.6*10^{-19}$ Coulombs, the sign of the charge is incorporated into the equation), v is the electron velocity at time t, V_0 is the accelerating potential, and b is the gap width. Assuming no initial momentum, integration yields the electron's velocity with respect to time,

$$\therefore v = \frac{V_0}{bm} qt$$

and integrating again yields the electron's position, x, as a function of time,

$$\therefore x = \frac{V_0}{2bm} qt^2 \tag{2.16}$$

The transit time, t_r, for an electron crossing the gap is obtained from equation (2.16),

$$t_r = \sqrt{\frac{2b^2 m}{V_0 q}} \tag{2.17}$$

A more rigorous calculation, using corrections for relativity yields [40],

$$t_r = (mcb / V_0 q)\left[\left(1 + V_0 q / mc^2\right)^2 - 1\right]^{1/2} \tag{2.18}$$

where c is the speed of light. In the limit $V_0 q << mc^2$, this simplifies to equation (2.17). The picosecond demodulator normally operates with $V_0 << mc^2/q \approx 510$ kV, therefore equation (2.17) is an adequate approximation for t_r.

Next consider what happens when the photodiode-waveguide structure supports a microwave field described by

$$E_x = \frac{V_1}{b}\cos(\omega t + \phi)$$

As V_0 accelerates electrons from the cathode to the anode, the microwave field will also produce a force on the electrons. If the microwave field increases the electron's velocity, then energy will be transfered from the field to the kinetic energy of the electron. If, however, the microwave field retards the electron, then the electron will lose kinetic energy to microwave field. If V_1 is small compared to V_0 (so that the electron is not stopped), then the electron energy lost to the field is found to be,

$$\begin{aligned} W &= \int \vec{F} \cdot d\vec{r} \\ &= \frac{qV_1}{b}\int_0^{x=b}\cos(\omega t + \phi)dx \end{aligned} \tag{2.19}$$

Using (2.16) to produce a change of variables,

$$dx = \frac{qV_0}{bm}tdt$$

lets (2.19) to be formulated in terms of transit time,

$$\begin{aligned} W &= \frac{q^2V_1V_0}{b^2m}\int_0^{t_r} t\cos(\omega t + \phi)dt \\ &= \frac{q^2V_1V_0}{b^2m}\left[\frac{t_r\sin(\omega t_r + \phi)}{\omega} + \frac{\cos(\omega t_r + \phi)}{\omega^2} - \frac{\cos\phi}{\omega^2}\right] \end{aligned} \tag{2.20}$$

Inserting (2.17) into this result and regrouping yields,

$$W = 2qV_1\left[\frac{\sin(\omega t_r + \phi)}{\omega t_r} + \frac{\cos(\omega t_r + \phi)}{\omega^2 t_r^2} - \frac{\cos\phi}{\omega^2 t_r^2}\right] \tag{2.21}$$

This is the work done by a single electron on the microwave field. If N electrons cross the gap, the energy transfered to the microwave field becomes,

$$W_N = 2qVN[\cdots] \tag{2.22}$$

Therefore, the energy transfered by N electrons in time t is the power transfered, P_e,

$$\begin{aligned} P_e &= \frac{W_N}{t} = 2qV_1\frac{N}{t}[\ldots] \\ &= 2V_1\frac{Nq}{t}[\ldots] \\ P_e &= 2V_1 i[\ldots] \end{aligned} \tag{2.23}$$

where i is the average current across the gap.

Ignoring the constant coefficients in equation (2.23), the term in brackets is

$$\left[\frac{\sin(\omega t_r + \phi)}{\omega t_r} + \frac{\cos(\omega t_r + \phi)}{\omega^2 t_r^2} - \frac{\cos\phi}{\omega^2 t_r^2}\right] \tag{2.24}$$

where the field phase angle, ϕ, indicates the phase of the microwave field during its interaction with the electron beam. In the limit where the transit time is short compared to the microwave field period, i.e., $\omega t_r \approx 0$, maximum power transfer occurs when ϕ=0. Therefore, in the short transit time limit, equation (2.24) becomes,

$$\lim_{\omega t \to 0}\left[\frac{\sin(\omega t_r)}{\omega t_r} + \frac{\cos(\omega t_r) - 1}{\omega^2 t_r^2}\right] = 1 - \frac{1}{2} = \frac{1}{2} \tag{2.25}$$

and therefore, when transit time is negligible,

$$P_e = V_1 i \tag{2.26}$$

When the transit time is large (i.e., when $\omega t_r \gg 1$), corresponding to the electron interacting with many cycles of the microwave field, equation (2.24) is dominated by the sine term. In this limit, equation (2.23) yield,

$$P_e = 2V_1 i \frac{\sin(\omega t_r + \phi)}{\omega t_r} \tag{2.27}$$

Finally, note that when ωt_r is near 1, the electron interacts with the field over nearly one cycle. In this case the complete form of equation (2.23) must be used for accurate analysis.

2.3.3 Waveguide power flow based on Field Theory

To determine the power transfered from the electron beam to the microwave field, the microwave field in the guide must next be calculated. Consider the reduced height waveguide shown in fig. 2-7. Driven by an $\hat{x}$ directed electron beam at y=a/2, the waveguide will support primarily TE_{0n} modes where n is odd. For TE_{01} mode propagation, the cutoff frequency of this structure is

$$f_c > \frac{1}{2a}\frac{1}{\sqrt{\mu\varepsilon}} = \frac{c}{2a} \tag{2.28}$$

The microwave power propagating through the waveguide is calculated as,

$$P_{field} = \int_0^b \int_0^a \langle \vec{S} \rangle dx dy$$

$$= \frac{abE_1^2}{4Z_0}$$

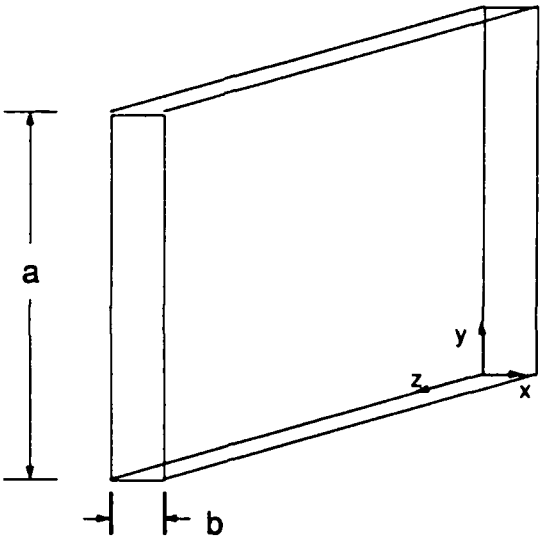

Fig. 2-7. Reduced height waveguide. The term "reduced height" implies b«a. This definition is for a geometry supports a TE_{01} mode with the electric field vector directed across the narrow gap (regardless of actual waveguide orientation in space).

$$P_{field} = \frac{bV_1^2}{4Z_0 a} \tag{2.29}$$

where $\langle \vec{S} \rangle$ is the time average time average Poynting power flow (a function of position) and Z_0 is the waveguide impedance defined by $|E_y|/|H_x| = \omega\mu/k_z$.

If a stub is placed a quarter wavelength from the driving source, as shown in fig. 2-8, then the $-\hat{z}$ field will add constructively to the $+\hat{z}$ field. The total field power propagating from one end of the waveguide will be,

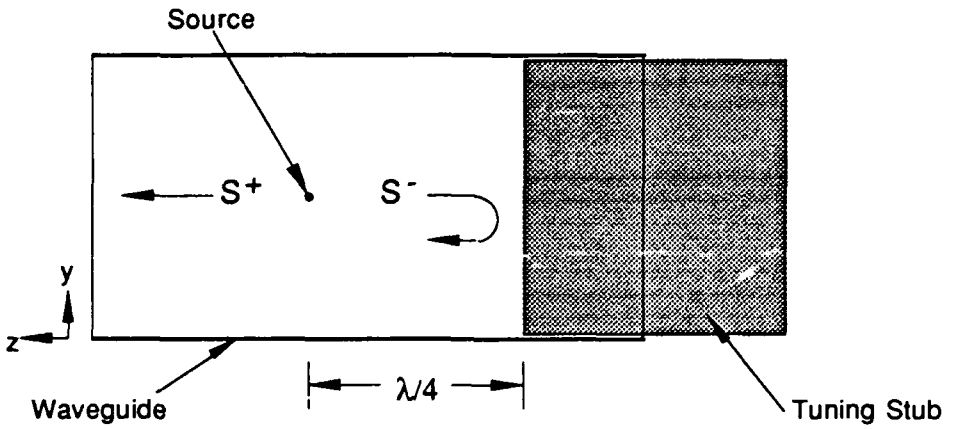

Fig. 2-8. Waveguide with stub a quarter wave from source. In this configuration the stub acts as a total reflector so that the negatively propagating wave is coupled out of the waveguide.

$$P_{wg} = \frac{bV_1^2}{2Z_0 a} = \frac{V_1^2}{R} \tag{2.30}$$

where $R=2Z_0a/b$.

If the drive current is modulated at a frequency ω, it is possible to excite and drive a TE_{01} mode in the waveguide. In this case, combining the electron beam power calculation from (equations (2.26) and (2.27)) and the waveguide power calculation from (equation 2-30), the total energy transfered from the electron beam to the TE_{01} field is calculated. In the limit where $\omega t_r \approx 0$, equations (2.26) and (2.30) are combined to yield,

$$\omega t \approx 0 \Rightarrow \qquad V_1 i = \frac{V_1^2}{R}$$

$$\therefore \qquad P_{wg} = i^2 R \tag{2.31}$$

where $R=2Z_0a/b$.

In the limit where transit time is not negligible, equations (2.27) and (2.30) are combined to yield,

$$\omega t \gg 1 \Rightarrow \qquad 2V_1 i \frac{\sin(\omega t_r + \phi)}{\omega t_r} = \frac{V_1^2}{R}$$

$$\therefore \qquad P_{wg} = i^2 R' \tag{2.32}$$

where

$$R' = \left(\frac{2\sin(\omega t_r + \phi)}{\omega t_r} \right)^2 R \tag{2.33}$$

Again, care must be exercised when using these approximations. As discussed above, when ωt_r is neither very large or very small, equation 2-24 must be used in place of the term in parentheses in equation (2.33),

$$R'=4(...)^2R \tag{2.34}$$

Assuming V_1 is constant for all ω, the rolloff of (2.33) and (2.34) is shown in fig. 2-9.

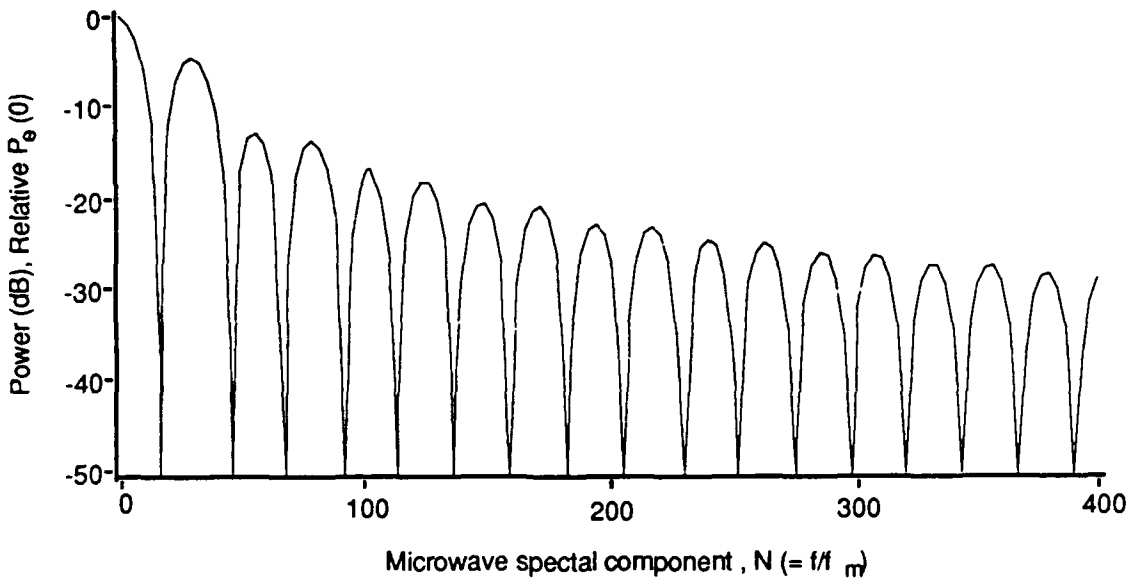

Fig. 2-9. Frequency response of the picosecond demodulator This graph was made for an electron transit time, t_r, of 265 pS and a pulse period, f_m, of 82 MHz. Using these definitions, the argument, ωt_r, to the rolloff function, equation (2.23), equals the product of N and the constant term, $2\pi f_m t_r$.

2.4. Picosecond Demodulator System Design

The entire picosecond demodulator system is shown in Fig. 2-10. The phototube and microwave sections convert the picosecond pulse information from the time domain to frequency domain. The last block in the system which manipulates the frequency domain data to derive time domain information about the optical pulse. This block performs two functions. First, it compensates for the overall system response to yield the

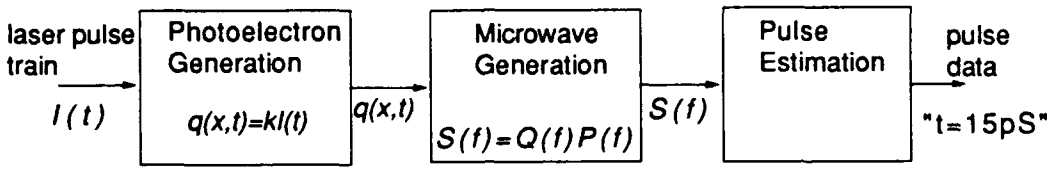

Fig. 2-10. Block diagram of the complete picosecond demodulator.

frequency domain representation of the laser pulse. Next, based on the frequency domain information, this section estimates the time domain parameters of the pulse.

The phototube converts the optical pulse to an electron pulse, so that,

$$q(x,t) = kI(t) \tag{2.35}$$

where $I(t)$ is the laser intensity profile, $q(x,t)$ is the charge density of the photoelectron bunch, and k is a conversion constant. In the frequency domain equation (2.35) is expressed as,

$$Q(f) = kI(f) \tag{2.36}$$

where $Q(f)$ and $I(f)$ are the Fourier transforms of the photocurrent and the laser pulse intensity. The microwave section output, $S(f)$, is the product of the photocurrent frequency domain spectrum, $Q(f)$ and the waveguide response, $P(f)$,

$$\begin{aligned} S(f) &= Q(f)P(f) \\ &= kI(f)P(f) \end{aligned} \tag{2.37}$$

In principle the parameter estimation block of the picosecond demodulator may obtain $I(t)$ by multiplying $S(f)$ by $\{kP(f)\}^{-1}$ and taking the inverse Fourier transform. (The inverse transfer function can be obtained from the impulse response of system.) These operations could be performed in real time by a digital computer, yielding the pulse profile $I(t)$. In practice, however, the hardware for sampling the microwave spectrum is limited in the range of frequencies it receives, generally sampling only a few microwave bands simultaneously. Although this restriction makes it difficult to obtain the complete pulse profile $I(t)$, it is possible to use the band sampled data to estimate the rolloff of a pulse of an assumed shape. Therefore, pulse width estimation becomes a simple problem of curve fitting.

2.5 Conclusion

This chapter has explained the theoretical principles of converting optical pulses to measurable microwave signals. Also considered was the general approach to calculating pulse width based on these measurements. These are the main ideas upon which the operation of the picosecond demodulator is based. The next chapter describes the hardware implementation of a picosecond demodulator and demonstrates that picosecond demodulation will work in principle for pulse width estimation.

Chapter 3

Experimental Design and Results

Based on the theories presented in the previous chapter, a prototype picosecond demodulator has been designed and tested. This chapter describes the picosecond demodulator design and its experimental performance (details of each experimental setup are presented in Appendix E). In the next chapter, the results of these experiments are analyzed and explained.

3.1 Picosecond Modulator Design

Based on the theoretical design of fig. 2-6, a prototype picosecond demodulator was built using a vacuum photodiode and a reduced height waveguide. The vacuum photodiode (ITT FW114A, see Appendix F), shown in fig. 3-1, has planar electrodes, S-20 spectral sensitivity, and is enclosed by a glass envelope. During experimental operation the diode bias was between 8 kV and 10 kV.

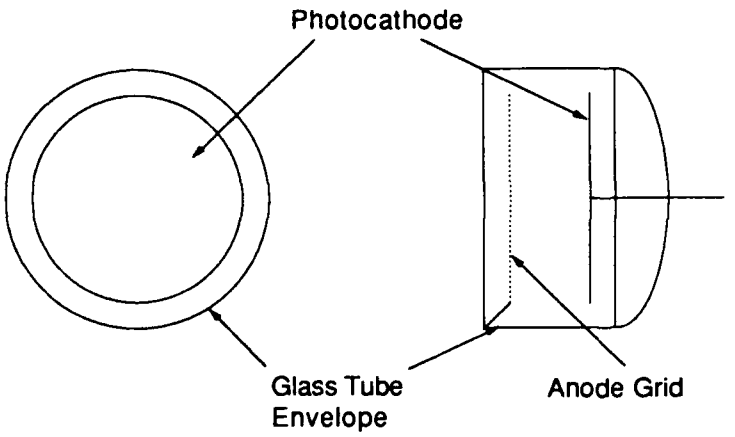

Fig. 3-1. Phototube geometry

The waveguide is a reduced height TE_{01} waveguide, with an opening to hold the phototube (fig. 3-2). The prototype waveguide was machined from aluminum in two pieces: a flat front plate and a slotted back. The front and back faces of the waveguide were made coplanar with the photodiode anode and cathode respectively. Together the phototube and the waveguide form a rectangular waveguide structure to propagate microwaves to the analyzer. The waveguide is terminated at one end by an movable aluminum plunger. The position of the plunger may be adjusted to obtain optimum microwave transmission from the open end of the waveguide. The complete picosecond demodulator design is shown in fig. 3-3.

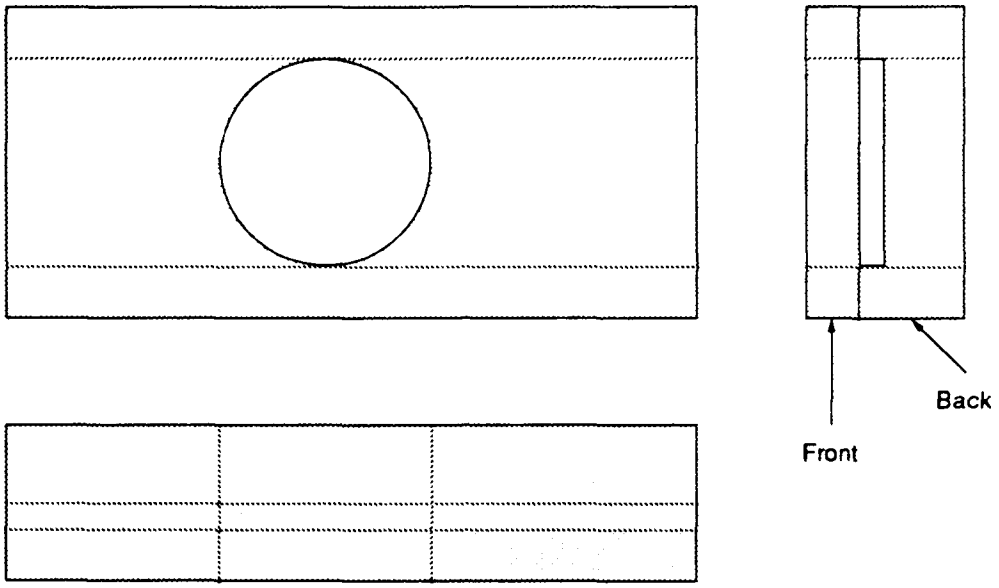

Fig. 3-2. Picosecond demodulator waveguide design. The circular hole was milled to hold the phototube. The rectangular waveguide was milled so that the front and back are parallel to the phototube electrodes.

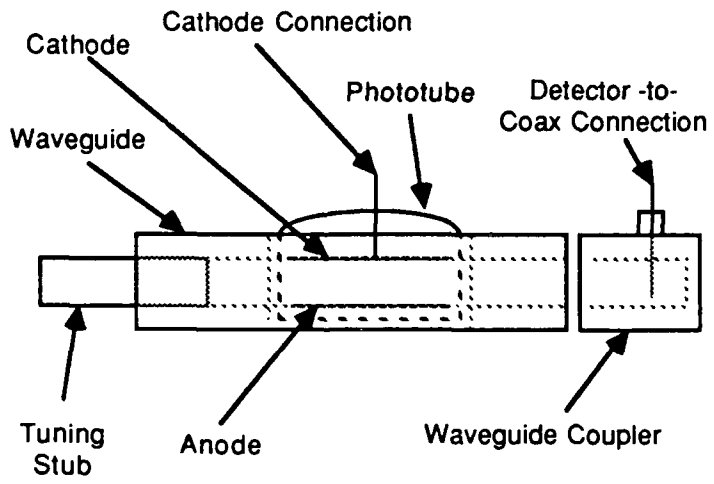

(a)

Fig. 3-3. Phototube and waveguide layout. a) Top view of device.

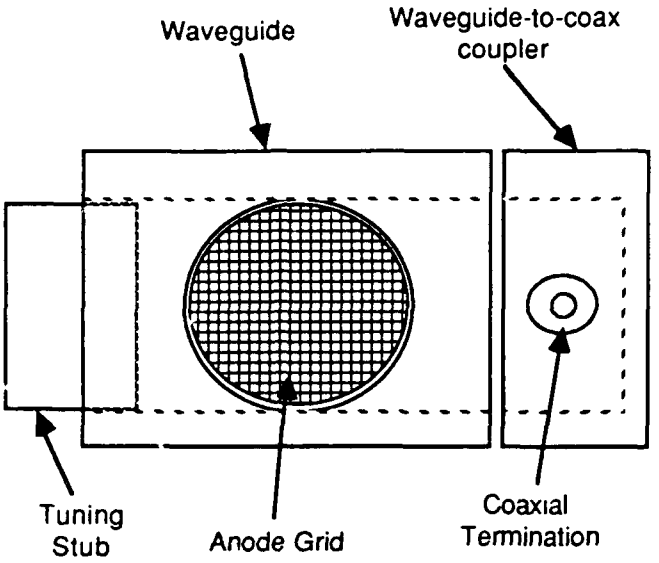

(b)

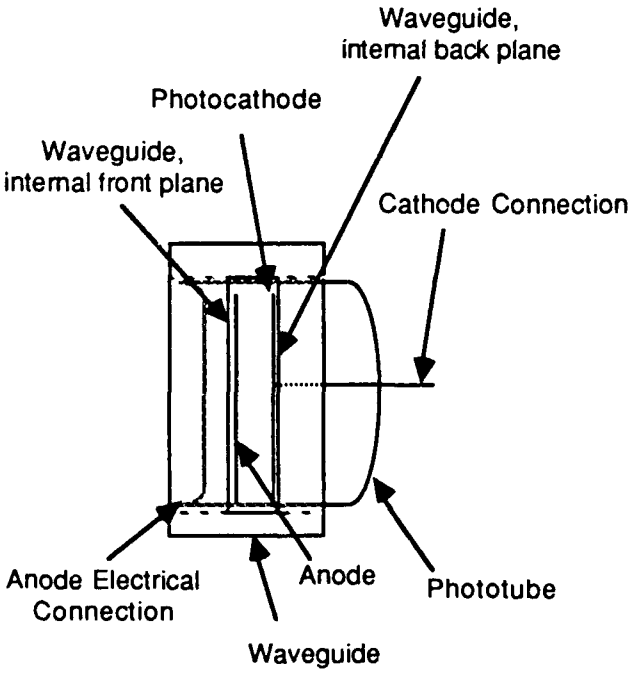

(c)

Fig. 3-3. Continued: b) Front view and c) side view of picosecond demodulator.

The phototube anode and the waveguide are connected together electrically and brought to ground through a resistor (approx. 100K ohms). The voltage drop across the resistor provides an easy means of monitoring the phototube current. The photocathode is biased by an adjustable high voltage supply.

In actual operation, the output signal from the phototube and waveguide assembly is the microwave spectrum of the optical pulse multiplied by the frequency response of the demodulator (equation 2.37). Three experimental approaches have been used to measure the microwave spectrum. First, a spectrum analyzer was used to capture and measure the microwave spectrum. The second approach used a microwave crystal detector to sample a narrow band of the microwave spectrum. Finally, a commercial multiband radar detector was used to sample the spectrum. The details of these experiments are discussed below.

3.2 General Experimental Layout

The general experimental setup is shown in fig. 3-4. The picosecond laser pulses for this work were generated using a synchronously pumped picosecond dye laser. The pulse duration of this type of laser can be controlled by changing the pump laser mode lock frequency or by changing the length of the dye laser cavity. For all experiments described here, the mode lock frequency was used to control the pulse length. The actual pulses were monitored using a commercial autocorrelator. Pulses were also routed to the picosecond demodulator using a beam splitter or removable mirror. This design allowed easy comparison between the output of the autocorrelator and the picosecond demodulator. (A detailed description of the laser system is found in appendix B.)

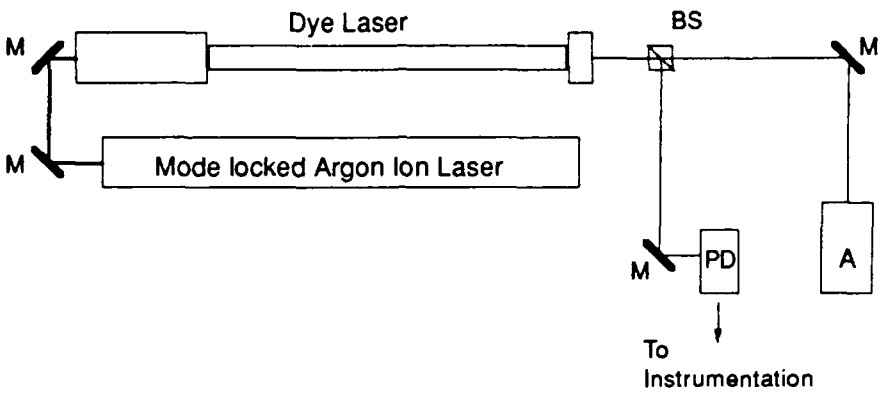

Fig. 3-4. Experimental layout for testing the picosecond demodulator M, mirror; BS, beam splitter; PD, picosecond demodulator; A, autocorrelator.

3.3 Experiment 1 - Broadband Spectrum Measurement

In the first experiment, the output of the picosecond demodulator was coupled through an S-band (2.6-3.9 GHz) horn into a spectrum analyzer. The laser system was tuned for minimum pulse width of approximately 30 picosecond. The analyzer output is shown in fig. 3-5. Careful measurement indicates that the spacing between the indicated maxima is 1.72 GHz; the spacing between adjacent modes is approximately 82 MHz. The measurable microwave spectrum extended from 2.54 GHz to 8 GHz, although beyond 6.1 GHz much of the signal was lost in the noise floor. The photocathode was biased at 8 kV.

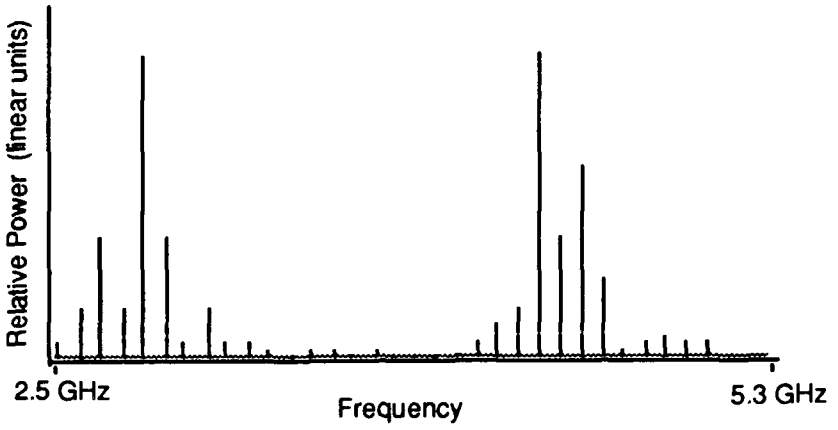

Fig. 3-5. S-band spectrum from picosecond demodulator The optical pulse width was 30 pS and the phototube bias was 8 kV.

3.4 Experiment 2 - Individual Spectral Component Analysis

The second experiment used the same spectrum analyzer setup, however the S-band horn was replaced by an X-band (8.2-12.4 GHz)waveguide to coaxial coupler. In this experiment the pulse width was varied by changing the mode lock frequency of the pump laser. The top row of images in fig. 3-6 shows the autocorrelator output as the mode lock frequency (and, hence, the pulse width) is varied. The autocorrelator was driven by 48 mW of average optical power. The second row of images in fig. 3-6, shows the spectrum analyzer output of a single frequency component (at 8.936 GHz) of the microwave spectrum; 15 mW of average optical power was incident on the phototube. The phototube bias voltage was 10 kV.

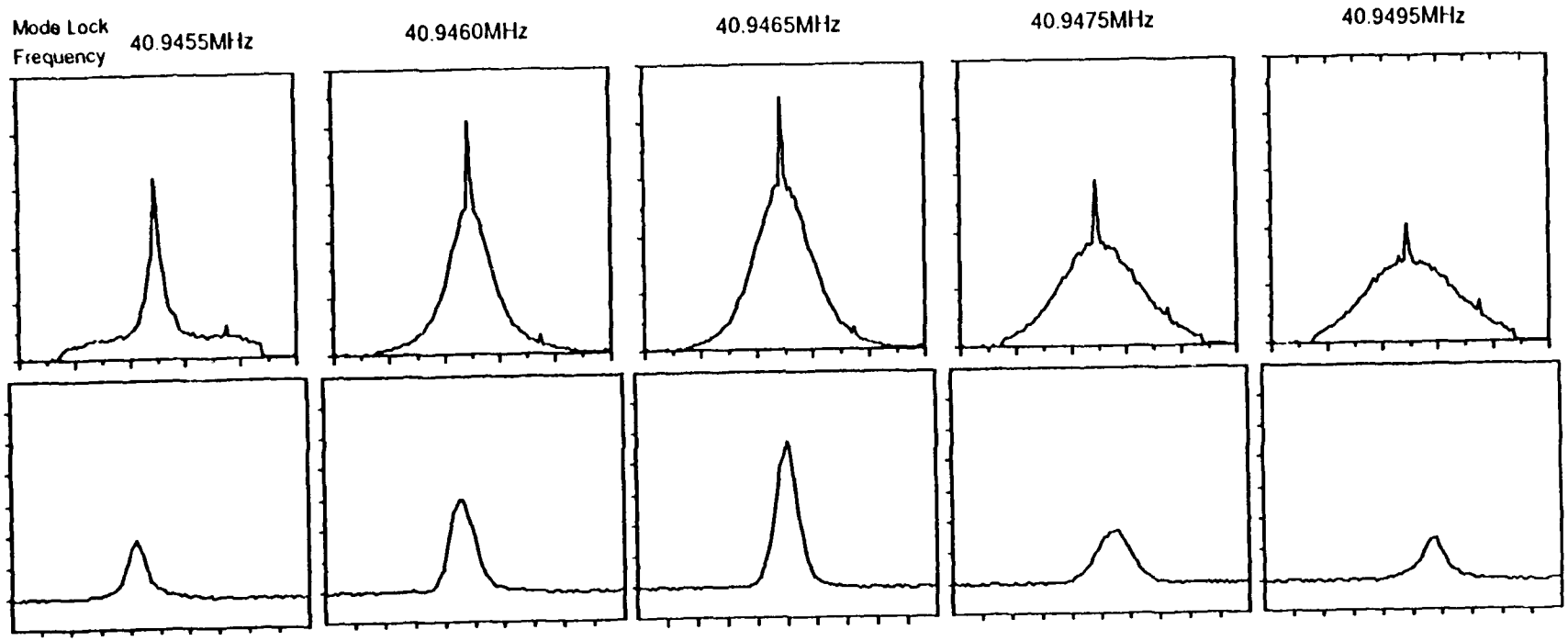

Fig. 3-6. Picosecond pulse width versus microwave line intensity. The top row is the autocorrelator signal, 15pS/div horizontally, relative intensity vertically. The bottom row is the spectrum analyzer output centered at 8.936GHz, .2MHz/div horizontally, relative amplitude vertically.

The broadband microwave spectrum passed by the X-band detector mound was found to extend from 7 GHz to 11.5 GHz, although many of the lines were obscured by noise. The detector was also found to be sensitive to microwaves emitted from the rear and face of the phototube.

3.5 Experiment 3 - Bandlimited Crystal Detector Response

In place of the spectrum analyzer, this experiment used a simple crystal detector (1N23) mounted in an X-band waveguide crystal mount. The detector output was amplified and fed to an oscilloscope. In this configuration the detector rectified the band limited microwave signal. The detector output was averaged by the low pass characteristic of the amplifier, therefore the oscilloscope display was proportional to the microwave power in the entire X-band.

The results of this experiment are shown in fig. 3-7. As in the last experiment the optical pulse width was varied by changing the pump laser mode lock frequency. The upper row of traces in fig. 3-7 shows the autocorrelator output as the mode lock frequency is varied. The lower row of traces shows the amplified detector output. (Note that the optical signal was chopped to provide a zero reference.) The phototube was biased at 10 kV and the average optical power incident on the photocathode was 7.5 mW. The amplifier provided a voltage gain of 1000 and had a cutoff above 300 Hz.

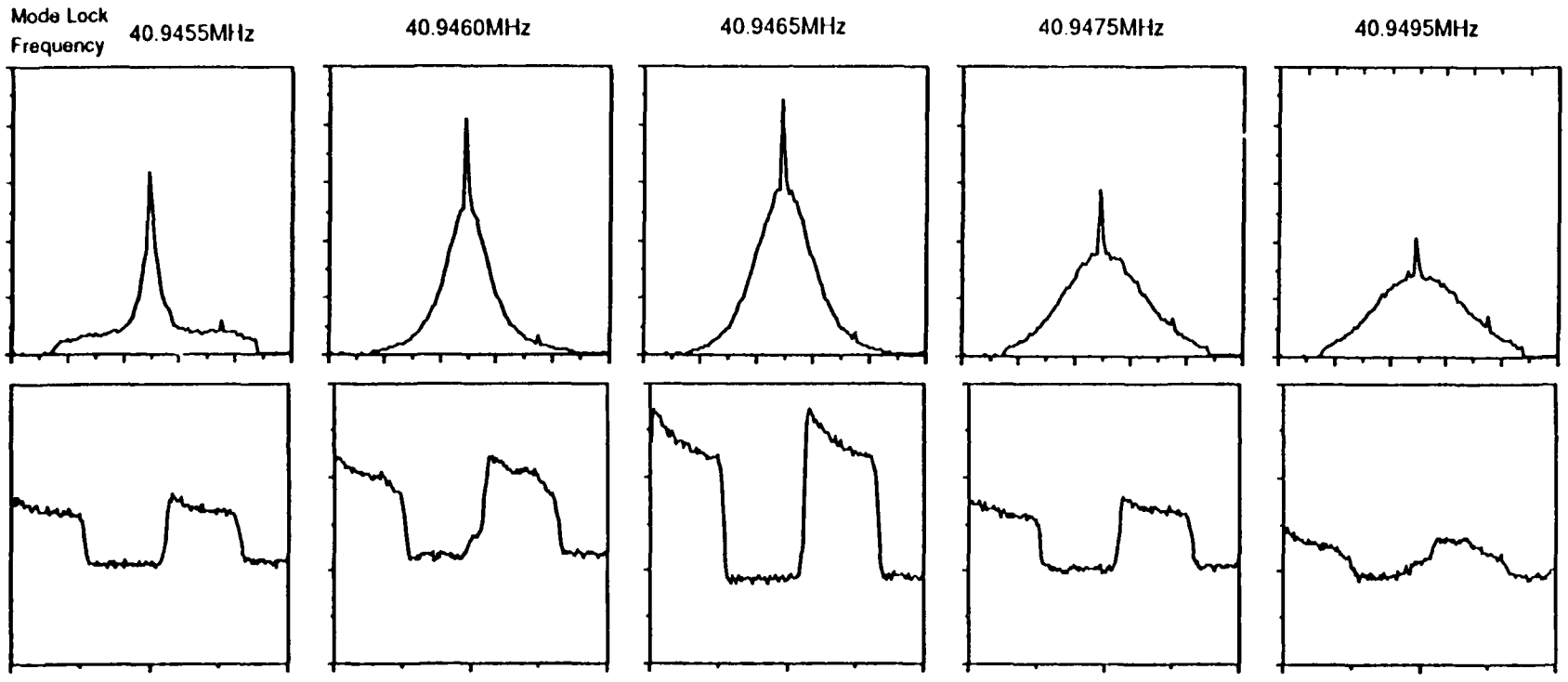

Fig. 3-7. Picosecond pulse width versus X-band energy The top row is the autocorrelator signal, 15pS/div horizontally, relative intensity vertically. The bottom row is the crystal detector output, 25ms/div horizontally, relative amplitude vertically.

3.6 Experiment 4 - Multiband Radar Detector Response

In the last experiment, the output of the picosecond demodulator waveguide was directed at an automotive radar detector (i.e., a "fuzzbuster"). The radar detector monitored microwave bands X (8.2-12.4 GHz), K (18-26.5 GHz), and Ka (26.5-40 GHz). The output of the radar detector was a set of five LEDs indicating relative detected power and three LEDs indicating the band with maximum signal. Pressing the reset switch caused the radar detector to switch bands.

When the picosecond demodulator was illuminated by 10 pS pulses (average power, 12 mW), the radar detector indicated microwave reception across all three bands. When the detector was 20 cm from the picosecond demodulator output, the power level for the X-band was greatest, with three LEDs illuminated. The K and Ka bands also showed microwave detection. When the radar detector was placed directly in front of the picosecond demodulator output slot, all five power level LEDs were illuminated for all three bands. When the picosecond demodulator was not illuminated, the radar detector registered neither K nor Ka power and only a single LED worth of X-band power.

As the optical pulse width was lengthened, the radar detector indicated a corresponding drop in microwave power. Concurrent with the increase of pulse width, there was also a drop in the average laser pulse power. Also, there appeared to be a slow drop in phototube current over time. This drop was corrected by turning off the high voltage supply for several minutes and then restarting the measurement.

Chapter 4

Discussion

This chapter uses the theory developed in chapter two to analyze the results reported in chapter three. First, the individual experiments are analyzed and the results are compared to the theoretical expectations. The overall success of the technique of picosecond demodulation is then discussed and future experiments proposed.

4.1 Experiment 1

The broadband spectrum obtained in the first experiment yields a good test of the microwave spectral rolloff. Assuming the picosecond pulse has a gaussian shape in time, the the frequency spectra of the pulse will also be gaussian. In the frequency band covered by the S-band, however, the frequency response will be approximately constant. Therefore, in the S-band the picosecond demodulator response will be dominated by the impulse response of the waveguide. For the S-band system described, ωt_r is much larger than one, hence, the microwave spectral rolloff due to the waveguide is predicted by equation (2.33), and is proportional to

$$\left(\sin(\omega t_r + \phi)/\omega t_r\right)^2 \tag{4.1}$$

where t_r is the electron transit time, ϕ is the interaction phase, and ω is the angular frequency of the microwaves. This equation will have maxima when,

$$\omega_m t_r = \frac{m\pi}{2} \quad \text{where } m \in \{1,3,5,\ldots \tag{4.2}$$

Therefore, the spacing between maxima is simply $\omega_r=\pi/t_r$. In terms of linear frequency, the maxima to maxima spacing is $f_r=1/(2t_r)$, or $t_r=1/(2f_r)$. Using this result, and the measurements made in the first experiment, the electron transit time is found to be approximately 265 pS. Based on an experimental phototube bias of 8 kV, and an electron transit distance of 6.5 mm, equation (2.17) yields an electron transit time of 246 pS. Within the error of the experimental system (e.g., high voltage supply calibration, photocathode geometry) these results are in reasonable agreement.

Figure 4-1 shows both the experimentally obtained spectrum and the theoretically predicted curve. Again, the empirical results provide a reasonable match to the theory that describes the rolloff function of the waveguide.

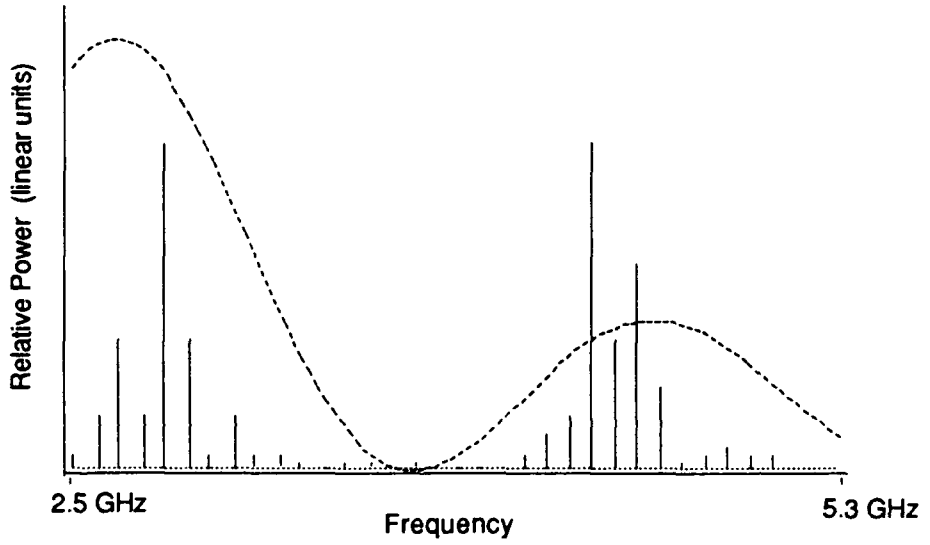

Fig. 4-1. S-band results and theory compared.

This experiment generally validates the theoretical analysis of the transfer of energy from the photoelectrons to the microwave field. The deviation of the experiment results, however, indicates that if the picosecond demodulator is used as a measurement device, then some type of calibration will need to be performed to compensate for variations in phototubes and voltage supplies. The deviations also indicate that the theoretical waveguide model may be too simple. Because the picosecond demodulator waveguide is closed by the microwave horn and the tuning stub, a rectangular cavity resonator may be a better system model.

4.2 Experiment 2

The most general result of experiment two is that at high microwave frequencies there is a strong correlation between the production of picosecond laser pulses and the intensity of individual microwave lines. This is a result predicted by Fourier theory because as pulses get shorter in time there must be a corresponding increase in the width of the frequency domain spectrum, and hence an increase in the intensity of the high frequency spectral lines (fig. 4-2). Therefore, the generation of strong high frequency microwave lines may be used as a diagnostic of a picosecond pulsed laser system. This idea is verified by this experiment, because we found that for day-to-day alignment and monitoring of the picosecond dye laser, the prototype picosecond demodulator gave an accurate indication of picosecond pulse production.

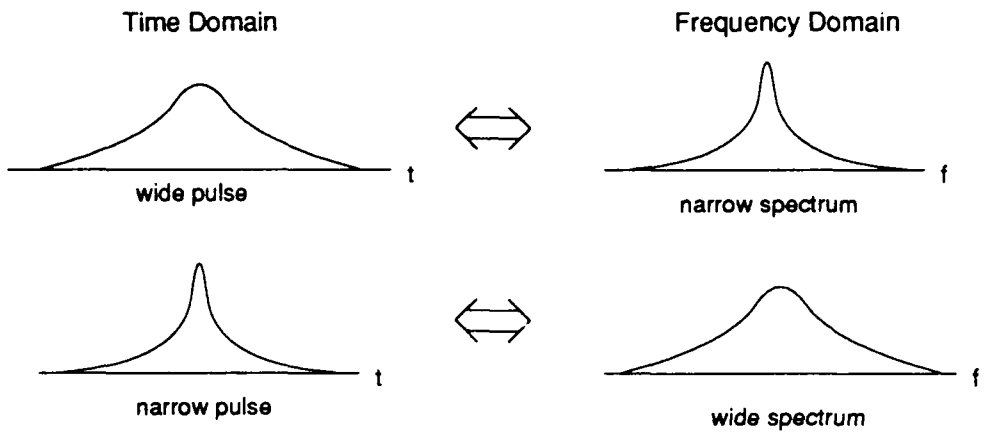

Fig. 4-2. Pulse width versus spectral width.

4.3 Experiment 3

In this experiment, the crystal detector produces an output that is proportional to the microwave power in the frequency band supported by the crystal mount. Because the detector signal is averaged by the response of the oscilloscope and the amplifier, the signal is proportional to the D.C. component of the rectified microwave frequencies. Therefore, as the optical pulse width decreases, the energy in the higher frequency microwave bands must increase and, hence, the D.C. level of the rectified signal in these bands should also increase. This is clearly seen in the results from this experiment. Shown in fig. 3-7 there is a strong correlation between decreasing optical pulse length and increasing power contained in the high frequency microwave components received by the X-band crystal mount.

Although not as sensitive as the spectrum analyzer used in the second experiment, the crystal detector system gave enough gain to be useful monitoring the production of picosecond laser pulses. This experiment also shows that fairly simple equipment yields a good laser system diagnostic.

4.4 Experiment 4

Although the measurements are crude, experiment four demonstrates a commercial radar detector has more than enough sensitivity to be used as a multi-band microwave detector. The major drawback with the commercial device was the meter interface. The LED display gave poor power resolution on only a single frequency band. A better interface would have three separate continuous signals corresponding to the power received in each band.

The gradual decrease in phototube current noted in this experiment may indicate that either the high voltage supply or the phototube is unstable. Further tests must be run to determine if the voltage drop is sensitive to the amount of optical power incident on the photocathode.

4.5 General Analysis

When compared to using an autocorrelator for routine laser monitoring, the picosecond demodulator has several advantages. First, the picosecond demodulator required little maintenance or alignment. The prototype required only crude (within 0.5 cm) alignment of the optical beam on the phototube, unlike the autocorrelator which requires total optical realignment whenever the input beam position is changed (e.g., due to minor changes in the laser mirror positions). The crystal detector demodulator used in

experiment three is also a relatively inexpensive device, with components costing less than $2000. This is comparable to the cost of other lab instrumentation, and quite inexpensive when compared to the cost of commercial autocorrelators or streak cameras. The most promising design is that of experiment four. The radar detector is inexpensive (≈$300) and provides multi-band reception of the waveguide output.

Also unlike the autocorrelator, the efficiency of the picosecond demodulator increases with decreasing wavelength. This is because at shorter spectral wavelengths, the process of photoemission becomes more efficient whereas frequency doubling becomes less efficient. (Not only does the doubling crystal efficiency drop, but attenuation at the doubled frequency by the detector windows also reduces the efficiency of the overall system.) Therefore, picosecond demodulation may be a useful technique for analyzing pulsed lasers operating in the blue and near ultraviolet.

Finally, because the picosecond demodulator generally requires a fraction of the laser output power for operation, it is possible to simultaneously run experiments and monitor the laser performance. This is especially useful for experiments where the laser may not have enough power to drive simultaneously a conventional measurement device and the experimental system.

The simple picosecond demodulator used in this work, however, has some limitations. First, the prototype picosecond demodulation is a severely limited diagnostic of the laser operation. Experiments one through three sampled at single frequency bands, hence, these preliminary devices provide only simple "go,no-go" measurements. A more useful tool would be one that provides an estimate of the pulse width and, possibly, an indication of the pulse shape. To produce such a measurement requires the sampling of

the microwave spectrum at two or more frequency bands. Experiment four moved in this direction, but , because of the crude meter output, accurate measurements could not be made. By modifying the radar detector circuitry it should be possible to obtain reasonable accurate band energy measurements. Then either the data could be fit to an assumed spectral shape (and hence yield pulse width) or the inverse Fourier transform of the data could be taken to yield both pulse shape and width.

Also unaddressed is the problem of cancelling the microwave system response and calculating the inverse Fourier transform of the microwave spectrum. It is believed that both these problems are best solved using computer software to calculate the inverse system response and the inverse Fourier transform. To determine the inverse system response requires either an accurate theoretical model of the system or accurate system calibration. The latter is the best approach to accurately account for individual system variations. By measuring the impulse response of the system (using a femtosecond pulsed CPM laser) the microwave detectors of the picosecond demodulator could be accurately calibrated across a bandwidth of several hundred gigahertz. Once the calibration information is obtained it is a simple matter to program a computer to analyze the data from real measurements.

Another potential limitation of picosecond demodulation is its ability to resolve picosecond and sub-picosecond pulses. A one picosecond pulse would have significant microwave components beyond 1000 GHz. At these frequencies however the attenuation of the picosecond demodulator (as extrapolated from Fig. 2-9 and equation (2-33)) would overwhelm any microwave signal. Therefore, to accurately demodulate picosecond pulses, the planar phototube must be replaced. De Lucia [25,26] has shown that slow wave structures improve the waveguide gain by a factor of 100. The work by

Defonzo et al. [30,31] suggests that a total solid state picosecond demodulator is possible and would have a response to a few terahertz. Integrating the antenna system with the microwave filters would yield an efficient, compact device.

The results from these experiments demonstrate that the principle of picosecond demodulation can be used to analyze ultrashort optical pulses. Although these experiments demonstrate some limitations in the prototype apparatus, accurate measurements appear possible with only minor system refinements.

Chapter 5

Conclusion

It has been 30 years since Forrester et al. [15] demonstrated that optical beats could be generated in the microwave. During much of this period, most research concerning optical beating and picosecond demodulation has been directed at development of alternative microwave sources. It is believed that the work discussed in this paper is the first application of picosecond demodulation for monitoring the characteristics of optical pulse trains.

This paper has developed the theory of picosecond demodulation and demonstrated its application for analyzing the microwave spectrum produced by picosecond laser pulses. In addition, the prototype demodulator provides a proof of principle that the technique of picosecond demodulation may be used to determine optical pulse characteristics.

As discussed in the previous chapter, pulse measurement by picosecond demodulation has inherent advantages and disadvantages. However, it is clear that the picosecond demodulator would make a useful supplement to the conventional autocorrelator for monitoring pulsed lasers systems. The prototype device demonstrates that a relatively simple instrument can be used to monitor laser pulse production. Using a modified radar detector, work is in progress to produce a calibrated demodulator for measuring pulse width. Work is also planned to develop an integrated solid state device and to extend the number of frequency bands sampled.

Finally, the application of picosecond demodulation is not limited to just the analysis of pulsed lasers outputs. Picosecond demodulation can be used to analyze any pulsed optical or electron beam device. One potential application is the analysis of the operating characteristics of a free electron laser. Free electron lasers (FEL) are driven by a beam of bunched electrons whose characteristics determine the laser output. It is desirable, therefore, to be able to monitor the electron beam without interfering with its propagation. Because the electron bunches are typically a few picosecond longs (comparable to the electron bunches generated by the lasers in this report), the technique of picosecond demodulation should be useful for monitoring the electron beam characteristics. By placing a picosecond demodulator between the alpha magnet of the FEL and the wiggler, the electron beam parameters could be monitored in real time. This application is currently being developed.

Appendix A

Fourier Transforms of Common Envelope Functions

The systems analysis approach can be used to convert real time domain pulse shapes to their frequency domain representations. This appendix demonstrates this approach for gaussian and hyperbolic secant envelopes.

Gaussian Envelope

A single optical pulse with a gaussian envelope (fig. A-1) is modelled as,

$$E(t) = g(t)\cos\omega_1 t \qquad \text{where } g(t)=\exp(-t^2/a^2) \qquad (A.1)$$

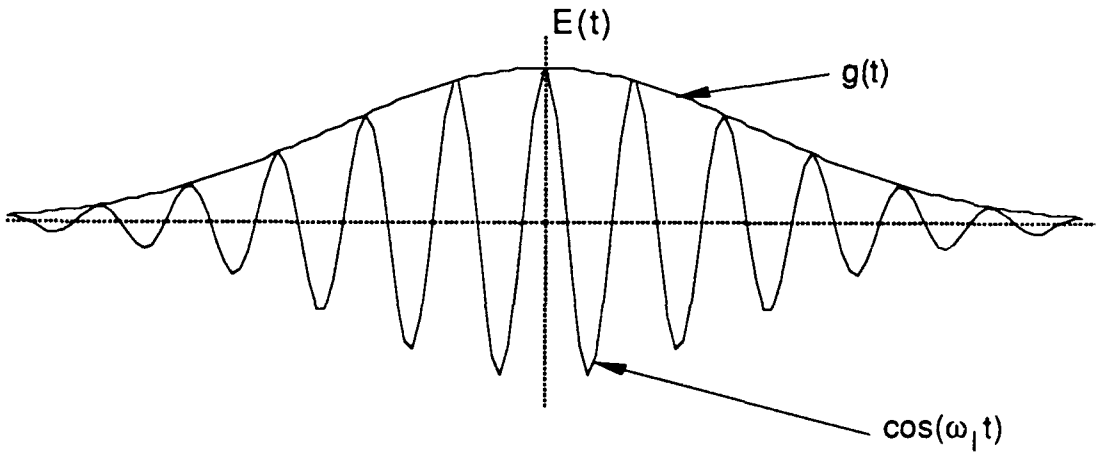

Fig. A-1. Gaussian envelope modulating a cosine carrier.

The Fourier transform of this envelope is,

$$G(\omega) = a\sqrt{\pi}\, \exp(-a^2\omega^2/4) \qquad (A.2)$$

The total transform of the original function is,

$$E(\omega) = G(\omega) \otimes (\delta(\omega+\omega_o) + \delta(\omega-\omega_o)) \qquad (A.3)$$

where $\otimes$ indicates the convolution operation.

Sech(t) and Sech^2(t) Envelopes

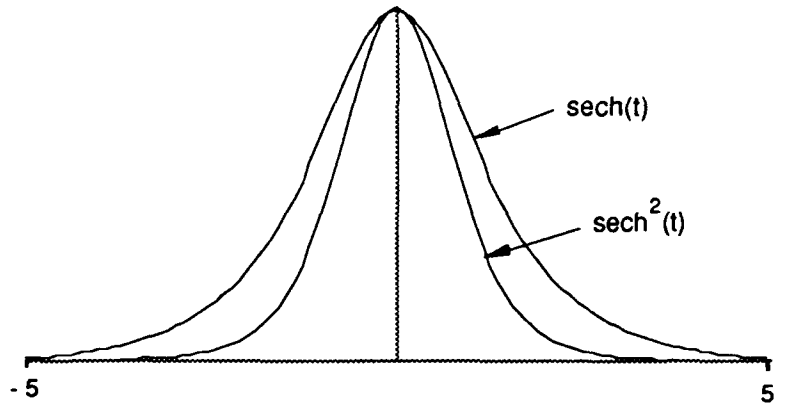

Fig. A-2. Profiles of Sech^2(t) and Sech(t).

Also found in the literature are pulses with sech^2(t) envelopes (fig. A-2). The spectrum of these pulses can be found by first considering the spectrum of a sech(t) pulse. Recognizing that sech(t) has only real Fourier transform components, the spectrum is found as,

$$G(\omega) = \mathrm{FT}\{\mathrm{sech}(t)\}$$

$$= \int_{-\infty}^{\infty} \frac{\cos(\omega t)}{\cosh(\omega t)} dt$$

$$= 2\int_{0}^{\infty} \frac{\cos(\omega t)}{\cosh(\omega t)} dt$$

$$G(\omega) = \pi \operatorname{sech}(\omega \pi/2) \tag{A.3}$$

Using the convolution property of Fourier transforms, the spectrum of $\operatorname{sech}^2(t)$ is found to be,

$$\mathrm{FT}\{\operatorname{sech}^2(t)\} = \pi^2[\operatorname{sech}(\omega\pi/2) \otimes \operatorname{sech}(\omega\pi/2)]$$

$$= \pi^2 \int_{x=-\infty}^{\infty} \operatorname{sech}(x\pi/2)\operatorname{sech}((x-\omega)\pi/2)dx \tag{A.4}$$

where $\otimes$ denotes the convolution operation. Transforming varibles of integration, $u=\omega\pi/2$, yields,

$$= 2\pi \int_{u=-\infty}^{\infty} \operatorname{sech}(u)\operatorname{sech}(u-\omega\frac{\pi}{2})du \tag{A.5}$$

$$= 2\pi \int_{u=-\infty}^{\infty} \frac{2}{\cosh(2u-a)+\cosh(a)} du \tag{A.6}$$

where the substitution $a=\omega\pi/2$ has been used. Changing variables again, yields,

$$= 2\pi \int_{v=-\infty}^{\infty} \frac{dv}{\cosh(v)+\cosh(a)} \tag{A.7}$$

where $2u\text{-}a=v$. This is a tabluated integral, solved by,

$$= 2\pi \frac{1}{\sqrt{\cosh^2(a)-1}} \left[\ln\left(\frac{e^x + \cosh(a) - \sqrt{\cosh^2(a)}}{e^x + \cosh(a) + \sqrt{\cosh^2(a)}} \right) \right]_{x=-\infty}^{\infty}$$

Restoring the original variables, yields

$$\mathrm{FT}\left\{\mathrm{sech}^2(t)\right\} = \frac{2\pi^2\omega}{\sinh(\omega\pi/2)} \tag{A.8}$$

Appendix B

Experimental Laser Description

The work covered in this paper used a synchronously pumped picosecond dye laser. The pump laser was an actively mode locked argon ion laser (Spectra-Physics 171). The laser cavity beam was mode locked using an acousto-optical Bragg defraction modulator (Spectra-Physics 342) to produce 200 pS wide optical pulses every 12.5 nS. These pulses pumped the dye laser gain media.

The dye laser (Spectra-Physics 375) used in this experiment used a three mirror folded cavity, extended to match the length of the pump laser. In the steady state the output of the dye laser produced pulses of approximately 15 ps every 12.5 nS (i.e., the period between pulses equals the mode lock period). Because the pulse is a travelling through a cavity that supports a standing wave, the relative phase difference of the optical carrier from pulse to pulse is zero. As a result the pulses emitted from the dye laser will have a high degree of pulse to pulse coherence.

The dye laser's wavelength of operation was selected by an adjustable tuning wedge in the dye laser cavity. The effect of the wedge is to limit the number of modes supported under the gain curve of the dye to a narrow band (fig. B-1). The dye laser used in this work had a typical line width of .3 nm.

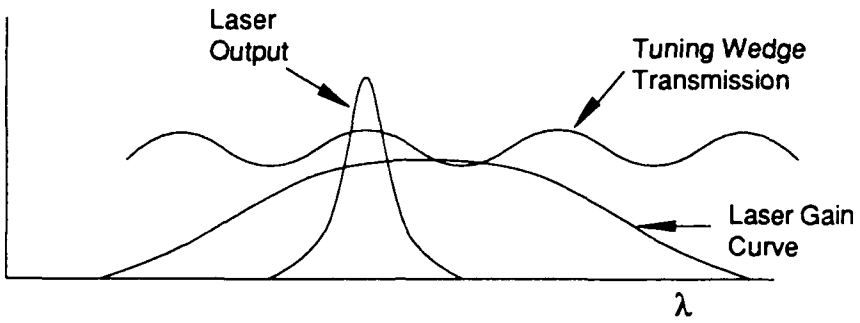

Fig. B-1. Laser mode selection by tuning wedge.

Appendix C

Work Function Effects on Electron Bunch Spreading

The second chapter discussed the generation and motion of electrons within the phototube. This discussion assumed that the electrons released from photocathode had no initial momentum. Einstein's photoelectric equation states [34], however, that the released electron will have an energy, K, equal to the difference between the work function of the cathode, p, and the energy, $h\nu$, of the photon,

$$K=h\nu\text{-}p. \tag{C.1}$$

Because of statistical variations in both the momentum of the electron before emission, and the penetration depth of the photon, the electrons emitted by the cathode will have a small variation in initial energies. Therefore, some electrons will travel faster and some will travel slower, the result being a spreading of the electron bunch.

This spreading can be calculated by solving the equations of motion for an electron (section 2.3.2) this time assuming an initial velocity, v_1, at the cathode:

$$F = \frac{d(mv)}{dt} = \frac{V_0}{b}q$$

$$\therefore\ v = \frac{V_0}{bm}qt + v_1$$

$$\therefore\ x = \frac{V_0}{2bm}qt^2 + v_1 t$$

where m is the electron mass, q is the electron charge, V_0 is the accelerating potential, v_1 is the initial velocity of an electron, and b is the gap width. The complete transit time equation is now quadratic,

$$0 = \frac{V_0 q}{2bm} t_r^2 + v_1 t_r - b$$

and this equation is solved by,

$$\begin{aligned} t_r &= \frac{bm}{V_0 q}\left(\sqrt{v_1^2 + \frac{2V_0 q}{m}} - v_1\right) \\ &= \frac{b}{V_0 q}\left(\sqrt{m^2 v_1^2 + 2V_0 qm} - mv_1\right) \end{aligned} \tag{C.2}$$

Recognizing that the initial kinetic energy of the electron is defined by,

$$K = \frac{1}{2} m v_1^2 \tag{C.3}$$

then (C.2) can be rewritten in terms of K as,

$$t_r = \frac{b}{V_0 q}\left(\sqrt{2Km + 2V_0 qm} - \sqrt{2Km}\right) \tag{C.4}$$

The variation in electron transit time, Δt_r, due to the variation in initial energy, ΔK, of the emitted electrons is now found by taking the first derivative of (C.4),

$$\Delta t_r = \frac{b}{V_0 q}\left\{m(2Km + 2V_0 qm)^{-1/2} - m(2Km)^{-1/2}\right\}\Delta K \tag{C.5}$$

As an example, the S-20 photocathode (CsNaKSb surface) used in this project has a work function of approximately 1.5 eV [43]. At the optical wavelength of 600 nm

(≈2 eV), the electrons may have an initial kinetic energy from 0 to 0.5 eV. Assuming the following experimental values,

$$q = 1.6*10^{-19}\text{C}$$

$$m = 9.1*10^{-31}\text{kg}$$

$$V_0 = 10\text{kV}$$

$$b = 6*10^{-3}\text{m}$$

equation (C.5) can now be evaluated for an average initial energy, K=0, and an energy spread ΔK=0.5 eV=.8*10^{-19} joules,

$$\begin{aligned}\Delta t_r &= \frac{bm}{V_0 q}(2V_0 qm)^{-1/2}\Delta K \\ &= 5*10^{-15}\text{seconds} \\ &= 5\text{ fs}\end{aligned}$$

From chapter four the transit time was found to be approximately 265 picoseconds. Therefore, for the experiments discussed in this paper, initial energies at the photocathode produce negligible electron bunch spreading.

Appendix D

Space charge spreading calculation

By making reasonable approximations it is possible to show that space charge spreading has negligible effect on the electron bunches in the phototube of the picosecond demodulator. This analysis starts by finding the charge in each bunch. A reasonable geometry for the charge distribution is then assumed allowing the use of Gauss' Law to determine the electric field produced by the charge bunches. The position of maximum field strength is then determined and this value is used to calculate the force and motion of a test charge. Finally, the equations of motion are used to determine the bunch deformation.

The amount of charge in bunch is found by measuring the average phototube current, calculating the average charge per unit time, and dividing this into the number of bunches per unit time. Therefore, each bunch contains a total charge, q,

$$q=Q/n=It/n \tag{D.1}$$

where Q is the average charge in the stream of bunches, I is the average photocurrent, n is the number of bunches in a time period t. Using data from experiment four, the charge per bunch is

I=0.02 mA t=1 second n=82*10^6 bunches/second

q≈0.25*10^{-12} Coulomb per bunch

The laser pulses have a time profile that is approximately gaussian in shape. At the photocathode, the time profile of the optical pulse is converted into an electron bunch with corresponding spatial profile. Therefore, the electron bunches will have a spatial profile along one axis that is approximately gaussian in shape,

$$q(x) \approx b\exp(-x^2/a^2). \tag{D.2}$$

The value for a is found by knowing τ, the full width at half maximum (FWHM) of the optical pulse. For an optical pulse width of 15 pS, a is approximately 2.7 mm.

Along the orthogonal axes, the bunch profile is defined by the spatial profile of the laser. This profile is also gaussian, with a full width at half maximum (FWHM) of approximately 3 mm. Because the geometries are similar, the analysis is simplified by assuming a spherically symmetric gaussian profile for the charge density function, $q(r)$, describing the electron bunch ,

$$q(r) = \exp(-r^2/a^2) \tag{D.3}$$

Integrating (D.3) over the entire volume of the charge bunch must yield the total charge in the pulse, therefore b is found as,

$$b = \frac{q}{4\pi \int_{r=0}^{\infty} r^2 \exp(-r^2/a^2)dr} = \frac{q}{3\pi^{3/2}a^3} \tag{D.4}$$

Using the values for a and q, b is found to be approximately $0.2*10^{-7}C/m^3$.

The electric field produced by the charge bunch can be found using Gauss' Law,

$$\oint_A \vec{D} \cdot d\vec{a} = \int_v \rho_v dv \tag{D.5}$$

which in spherical coordinates yields,

$$4\pi r^2 \varepsilon \vec{E}(r) = \int_V \rho_v dv \tag{D.6}$$

Substituting the assumed charge distribution function, the electric field is

$$\vec{E}(r) = \frac{b}{\varepsilon r^2} \int_{r'=0}^{r'=r} r'^2 \exp(-r'^2 / a^2) dr' \tag{D.7}$$

The position of maximum field is found when the first derivative of (D.7) equals zero. Performing this calculation, E_{max} occurs when $r=a$. At this position the charges will feel the greatest force from the electric field produced by the space charge density. Calculated numerically, the electric field at $r=a$ is,

$$\vec{E}(r = a) = 200 \frac{\mathrm{V}}{\mathrm{m}} \tag{D.8}$$

Assuming the charge distribution is initially fixed, the motion of an individual charge can be found by solving the equation of motion,

$$F = m\frac{d^2x}{dt^2} = Eq \tag{D.9}$$

where m is the rest mass of the electron. Solving (D.9) for x yields,

$$x(t) = \frac{Eqt^2}{2m} \tag{D.10}$$

From the transit time calculation in chapter four, the electron bunches exist for approximately 300 ps. Using this value for t, and inserting the calculated value of the maximum electric field for E, space charge effects produce a maximum displacement change of approximately 10^{-7} meters. Because this change in pulse shape is much

smaller than the overall pulse size ($\approx 3*10^{-3}$ m), space charge effects at the low currents used in this research can be considered negligible.

Appendix E

Experimental Equipment List

This section lists the equipment used in this research and the associated experiments.

Pump Laser: Spectra Physics 171 Argon Ion Laser with a Spectra Physics 452 Mode Lock Driver running single line at 514 nm. Mode lock frequency, ≈ 40.9545 MHz; mode locked laser output power ≈ 0.7W.

Dye Laser : Spectra Physics 375 with extended cavity, Rhodamine 6G running at 595 nm.

Autocorrelator: Spectra Physics 409.

Phototube: ITT FW 114A, biased at 10 kV.

Spectrum Analyzer: HP 8555A RF, HP 8552B IF, HP 8445B Preselector

Crystal Detector: Sylvania 1N23

Radar Detector: Bel Vector 3 Radar Detector, manufactured by Bel-tronics, 20 Centre Drive, Orchard Park, NY, 14127.

Appendix F

ITT 114A Specifications

FW114A

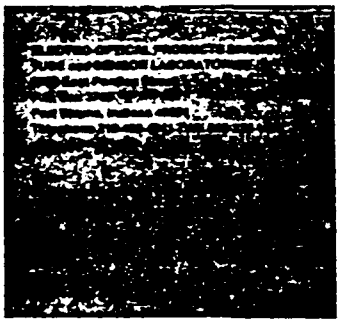

1435

BIPLANAR PHOTOTUBE

- Fast Picosecond Response
- Biplanar Geometry
- Ultra-linear
- Wide dynamic range
- Calibration Standard Dependability
- Damage Resistant Long-Life
- Broad Spectral Response
- Low Impedance Photocathode
- Coaxial Output

GENERAL DESCRIPTION

The FW114A is a 2¼-inch diameter high vacuum photodiode with an opaque photocathode having an S-20 type spectral response. (See Note 7.) Visible light transmitting glass is used for the entrance window. The FW114A was developed by ITT specifically for laser detection applications such as the investigation of fundamental laser properties, laser communications systems, and laser radar systems.

The plane parallel (biplanar) and coaxial electrode geometry combined with high voltage ratings, low dark current, and red response extending beyond 7000Å make the FW114A particularly valuable for the detection and monitoring of high energy pulsed ruby laser radiation. Linear output currents exceeding 5 amperes can be delivered to a terminated coaxial cable with a rise time of less than 5×10^{-10} seconds. The radiant energy spectrum of the laser generator can be examined in detail over a minimum of 9 orders of magnitude in intensity within the gigacycle frequency range.

The FW114A is one of a family of biplanar phototubes available from ITT. Three other biplanar type photodiodes are the 2¼-inch diameter FW114, the 1⅛-inch diameter FW128, and the 5-inch diameter FW127. Information on several other types under development is available on request.

FW114A

FW114A TENTATIVE DATA

1435 f

Over-all length	47.5 mm (1.870 in.) max
Over-all diameter	58.0 mm (2.284 in.) max
Weight	63.79 g (2.25 oz)
Photocathode to anode spacing	6.4 mm (0.250 in.) nominal
Effective photocathode diameter	44.5 mm (1.75 in.) nominal
Effective photocathode area	15.5 cm^2 (2.4 sq. in.) nominal
Window diameter	44.5 mm (1.75 in.) nominal
Anode mesh (Note 1)	20 openings/25.4 mm (1 in.)
Anode mesh transmission	80 percent, typical
Resistance of anode mesh	0.5Ω per square, typical
Operating voltage	2.5 kV, typical
Photocathode spectral response (Note 7)	S-20
Photocathode luminous sensitivity (Note 2)	80 μA/lm, typical
	50 μA/lm, min.
Photocathode peak radiant sensitivity (Note 3)	0.034 A/W, typical
Maximum peak current output (Note 4)	5 A
Maximum average current output (Note 5)	100 μA
Deviation from linearity (Notes 4 & 6)	± 10 percent, max.
Dark current (Note 4)	2.5×10^{-10} A, typical
	5×10^{-9} A, max
Interelectrode capacitance	7 pF, typical
Rise time	5×10^{-10} sec, max.

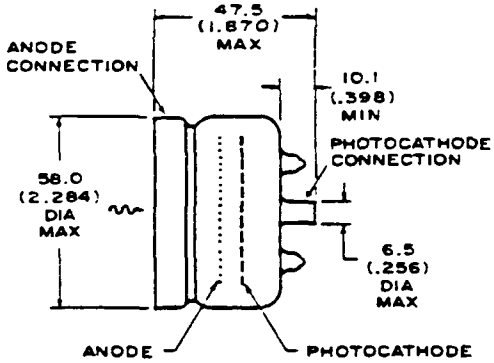

DIMENSIONS IN mm (in)

BIPLANAR TYPE PHOTOTUBE FW114A

NOTES:

1. Electroformed nickel.
2. 2870 degrees K color temperature tungsten radiation incident on faceplate. Two-hundred volts anode potential.
3. Calculated from the approximate relationship: peak radiant sensitivity in amperes per watt equals 4.3×10^{-4} times the luminous sensitivity in microamperes per lumen, this relationship being derived from a typical S-20 spectral response peaking at 4200 Å.
4. At 2.5 kV.
5. Output current averaged over a 1-second time interval and uniformly distributed over the photocathode. For lower operating voltages the permissible output current will be reduced according to the usual three halves power law of applied voltage.
6. Deviation from direct proportionality between current output and light flux input uniformly distributed over the photocathode.
7. The S-20 designation is for a multi-alkali photosurface on a transluceent glass substrate. The FW114A photocathode is formed on an opaque metal substrate. Therefore, there may be a departure from the typical S-20 spectral response curve.

Rev. 10-75

ELECTRO-OPTICAL PRODUCTS DIVISION ITT
3700 E. Pontiac St., Fort Wayne, Ind. 46803

References

[1] A.J. DeMaria, C.M. Ferrar, G.E. Danielson, " Mode locking of a Nd^{3+}-doped glass," Appl. Phys. Lett. **8** 22-24 (1965).

[2] C.V. Shank, "Generation of Ultrashort Optical Pulses," in Ultrashort Laser Pulses and Applications , ed. W. Kaiser (Berlin: Springer-Verlag, 1988), 5-34.

[3] R.L. Fork, C.H. Brito Cruz, P.C. Becker, C.V. Shank, "Compression of optical pulses to six femtoseconds by using cubic phase compensation," Opt. Lett., **12** 483-5 (1986)

[4] A.E. Siegman, Lasers, (Mill Valley, CA: University Science Books, 1986).

[5] A. Valdmanis, R.L. Fork, J.P. Gordon, "Generation of optical pulses as short as 27 femtoseconds directly from a laser balancing self-phase modulation, group-velocity dispersion, saturable absorption, and saturable gain," Opt. Lett. **10** 131-3 (1985).

[6] P.M.W. French, J.R. Taylor, "Femtosecond Pulse generation from passively mode locked continuous wave dye lasers 550-700nm," in Ultrafast Phenomena V (Springer series in Chem. Phys. vol. 46) ed. G. Fleming and A.E. Siegman, (Berlin:Springer, 1987), 11-13.

[7] M.L. Skolnik, Introduction to Radar Systems, (New York: McGraw-Hill, 1962), 493-8.

[8] M.R. Baggs, R.T. Eagles, W. Margulis, W. Sibbett, W.E. Sleat, "Subpicosecond Chronoscopy Using a Photochron IV Sreak Camera," in Advances in Electronics and Electron Physics (vol. 64B, Photoelectronic Image Devices), ed. B.L.Morgan (London: Academic Press 1985).

[9] K.Kinoshita, M. Ito, Y. Suzuki, "Femtosecond streak tube," Rev. Sci. Instrum. **58** 932-8 (1987).

[10] S. Majumdar, P.Y. Key, M. Yaschelev, Y. Surdyuchenko, W. Seka, M.C. Richardson, P. Yaanimagi, R. Keck, "Evaluation of PV001 and P-100 Tubes for Muliple channel Streak Cameras," in Advances in Electronics and Electron Physics (vol. 74, Photoelectronic Image Devices) ed. P.W. Hawkes, (London: Academic Press, 1988).

[11] R.J. Seymour, R.R. Alfano, "Time resolved measurement of the electron spin relaxation kinetics in GaAs," Appl. Phys. Lett. **37** 231-3 (1980).

[12] A.G. Doukas, J. Buchert, R.R. Alfano, "Picosecond laser techniques and design," in Biological Events Probed by Ultrafast Laser Spectroscopy, (London: Academic Press, 1982), 387-415.

[13] J. Buchert, R. Dorsinville,P. Delfyett, S. Krimchansky, R.R. Alfano, "Determination of temporal correlation of ultrafast laser pulses using phase conjugation," Opt. Comm. **52** 433-7 (1985).

[14] J.A. Giordmaine, P.M. Rentzepis, S.L. Shapiro, K.W. Wecht, "Two photon excitation of fluorescence by picosecond light pulses," Appl. Phys. Lett. **11** 216-8 (1967).

[15] A.T. Forrester, R.A. Gudmundsen, P.O. Johnson, "Photoelectric mixing of incoherent light," Phys. Rev. **99** 1691-1700 (1955).

[16] A.T. Forrester, "Photoelectric mixing as a spectroscopic tool," J. Opt. Soc. Am. **51** 253-9 (1961).

[17] B.J. McMurty, A.E. Siegman, "Photomixing experiments with Ruby Optical Maser and a traveling-wave microwave phototube," Appl. Opt. **1** 51-3 (1962).

[18] B.J. McMurty, J.B. Gaenzle, A.E.Siegman, "Broadband detectors for microwave modulated light," journal unkown 434-439.

[19] M.D. Petroff, H.A. Spetzler,E.K. Bjørnerud, "X-band Microwave Phototube for demodulation of laser beams," Proc. IEEE, **51** 614-5 (1963).

[20] N.C. Wittwer, "Detection of higher order ruby optical maser modes," Appl. Phys. Lett. **2** 194-6 (1963).

[21] A.E. Siegman, S.E. Harris, B.J. McMurty, "Microwave Demodulation of Light" in Proceedings of the third international congress of Quantum Mechanics, ed. P. Grivet, N. Bloembergen, (New York: Columbia University Press, 1964), 1651-8.

[22] A.M. Johnson, D.H. Auston, "Microwave switching by picosecond photoconductivity," IEEE J. Quan. Elec. **QE-11** 283-7 (1975).

[23] C. H. Lee, P. S. Mak, A.P. DeFonzo, "Optical control of millimeter-wave propagation in dielectric waveguides," IEEE J. Quan. Elec. **QE-16** 277-88 (1980).

[24] G. Mourou, C.V. Stancampiano, D. Bluementhal, "Picosecond microwave pulse generation," Appl. Phys. Lett. **38** 470-2 (1981).

[25] F.C. De Lucia, "The generation of near millimeter radiation by picosecond pulse demodulation," Night Vision and Electro-Optics Laboratory Report #DAAK 70-79-C-0121, Fort Belvoir, Virginia, (1983).

[26] F.C. De Lucia, B.D. Guenther, T. Anderson, "Microwave generation from picosecond demodulation sources," Appl. Phys. Lett. **47** 894-6 (1985).

[27] G. Arjavalingham, Y. Pastol, J.M. Halbout, G.V. Kopcsay, "Optoelectronically generated transient radiation for broadband microwave measurements," Conference

on Lasers and Electro-Optics, 1989 Technical Digest Series, Vol. 11 (Washington D.C.: Opt. Soc. Amer., 1989), 326.

[28] P.R. Smith, D.H. Auston, M.C. Nuss, "Subpicosecond photoconducting dipole antennas," IEEE J. Quant. Electr., **QE-24** 255-60 (1988).

[29] C. Fattinger, D. Grischkowsky, "Point source terahertz optics," Appl. Phys. Lett. **53** 1480-3 (1988).

[30] A.P. DeFonzo, M. Jarwala, C. Lutz, "Transient response of planar integrated optoelectronic antennas," Appl. Phys. Lett. **50** 1155-7 (1987).

[31] A.P. DeFonzo, C. Lutz, "Optoelectric transmissionand reception of ultrashort electric pulses," Appl. Phys. Lett. **51** 212-5 (1987).

[32] P.W. Smith, "Mode-locking of lasers," Proc. IEEE **58** 1342-57 (1970).

[33] W. Siebert, Circuits, Signals and Systems, (Cambridge: MIT Press, 1986).

[34] A.L. Hughes, L.A. DuBridge ,Photoelectric Phenomena, (New York: McGraw-Hill, 1932).

[35] V.K. Zworykin, E.G. Ramberg, Photoelectricity and its Application, (New York: Wiley, 1949), 8.

[36] W.E. Spicer, F. Wooten, "Photoemission and photomultipliers," Proc. IEEE, **51** 1119-26 (1963).

[37] A. Finch, Y. Liu, H. Niu, W. Sibbett, W.E. Sleat, D.R. Walker, Q.L. Yang, H. Zhang, "Recent Advances Towards a 100fs-Resolution Streak Camera," in Springer Series in Chemical Physics, vol. 48: Ultrafast Phenomena IV, ed. T Yajima et al. (Berlin: Springer-Verlag, 1988), 159-61.

[38] A.B. Bromwell, and R.E. Beam, Theory and Application of Microwaves, (New York: McGraw-Hill, 1947).

[39] R.F. Soohoo, Microwave Electronics, (Reading, MA: Addison-Wesley, 1971).

[40] D.J. Griffiths, Introduction to Electrodynamics, (Englewood Cliffs,NJ: Prentice-Hall, 1981), chapter 10.

[41] G.D. Sims, I.M. Stephenson, Microwave Tubes and Semicondutor Devices, Wiley New York, 1963, p.58.

[42] A. Yariv, Optical Electronics, 3rd ed., (New York:Holt Rinehart Winston, 1985).

[43] W. Spicer, "Photoemission and Related Properties of the Alkali-Antimonides," J. Appl. Phys. **31** 2077-84 (1960).

Biography

John C. Swartz [redacted] received his Bachelor's degree in Electrical Engineering from the Massachusetts Institute of Technology. From 1985 to August 1987 he worked for GenRad Inc. as a digital design engineer on the 2750 project. In September 1987, he entered the the Department of Electrical Engineering at Duke University. In the fall of 1989 he received his Master's Degree in Electrical Engineering. He is currently a member of the IEEE. Mr. Swartz has published the following papers:

"Application of Frequency Domain Techniques for Tuning Pulsed Lasers," J. Swartz, F. De Lucia, B. Guenther, Topical Meeting on Picosecond Electronics and Optoelectronics, 8-10 March 1989, Salt Lake City, UT, Optical Society of America.

Patent Pending, "A device for tuning pulsed lasers," F. De Lucia, B. Guenther, J. Swartz.